Coherent magneto-tunneling in double barrier structures : the B - J configuration

van Tartwijk, G.H.M.

Award date:
1990

COHERENT MAGNETO-TUNNELING IN DOUBLE BARRIER STRUCTURES; THE $\underline{B} \perp \underline{J}$ CONFIGURATION

G.H.M. van Tartwijk

DECEMBER 1990

Master's Thesis on theoretical work performed in the Theoretical Physics group of the Physics Department of the Eindhoven University of Technology

Supervisor: Prof. Dr. D. Lenstra
Coach: Ir. H.J.M.F. Noteborn

ABSTRACT

The I-V characteristic of a Double Barrier Resonant Tunneling structure is a strong peak of resonant current on a background of non-resonant current. The DBRT's behavior is explained by a model that describes the coherent interaction between emitter, quantum well, and collector in a selfconsistent way.

When B=0, the voltage interval in which resonant current exists coincides with the one of resonant charge build-up in the well.

When B≠0, two changes occur:

1. The two intervals shift and either broaden or contract.
2. The resonant current interval is now only a part of the charge build-up interval.

When B is increased, the resonant current interval contracts so fast that for a finite value of B, the *Killing Field*, its width is zero: for this value of B and higher no resonant current is possible.

This interesting effect is explained by the transformation of "Resonant States" into "Quasi-Bound States", induced by the magnetic field. These Quasi-Bound States contribute to the charge build-up but not to the resonant current, and are a manifestation of "skipping orbits".

CONTENTS

Dankwoord:

Bij deze wil ik Harry Noteborn en Daan Lenstra bedanken voor hun uitstekende en enthousiaste begeleiding tijdens de afgelopen negen maanden. Met name wil ik Harry bedanken voor zijn opgeofferde vrije zaterdagen/zondagen. GvT

INTRODUCTION

In 1969, research on semiconductor superlattices was initiated by a proposal by Tsu and Esaki [1], [2] for a one-dimensional potential structure "engineered" with epitaxy of alternating ultrathin layers. In anticipation of future technology, two types of superlattices were envisioned: doping and compositional. It is nowadays possible to prepare well defined, high purity, semiconductor layers, with a thickness as small as one atomic layer. These layers can be put together to form a heterostructure. The standard techniques available for growing such structures are molecular beam epitaxy (MBE) and metal-organic chemical vapor deposition (MOCVD).

A semiconductor is characterized by a band gap of typically 1.0 eV between conduction band and valence band. This band gap causes the semiconductor to behave sometimes as a conductor and sometimes as an insulator, dependent on the temperature and the density of strange elements (doping, impurities) in the semiconductor. The origin of this band gap lies in the wave character of electrons. For energies in the band gap, the electron wave functions interfere destructively with the lattice points of the semiconductor crystal.

The proposal of Tsu and Esaki was to create an additional periodicity for the electrons by means of periodically changing the energy gap between the lowest valence band and the lowest conduction band (ultrathin layers of different semiconductors). The potential structure thus created resembles a Kronig-Penney chain. Therefore they expected additional forbidden zones; these additional bands are called minibands.

The semiconductor compounds Gallium-Arsenide (GaAs) and Gallium-Aluminum -Arsenide (AlGaAs) are often used for this purpose because the difference in lattice constant is very small (the interfaces are very neat). However, it is still a problem to describe electrons at such an interface, because of the change in effective mass (boundary conditions) and local charge accumulation.

In this report we restrict ourselves to a socalled Double Barrier Resonant Tunneling structure (DBRT). Because of the limited periodicity (only two layers of AlGaAs in the GaAs), we do not expect minibands. The DBRT structure has some very interesting properties both in physics (fundamental quantum mechanical aspects) and electronics (as a device that could be used as a ultrafast switch). In Figure 1 the potential picture of a typical DBRT structure under bias is shown.

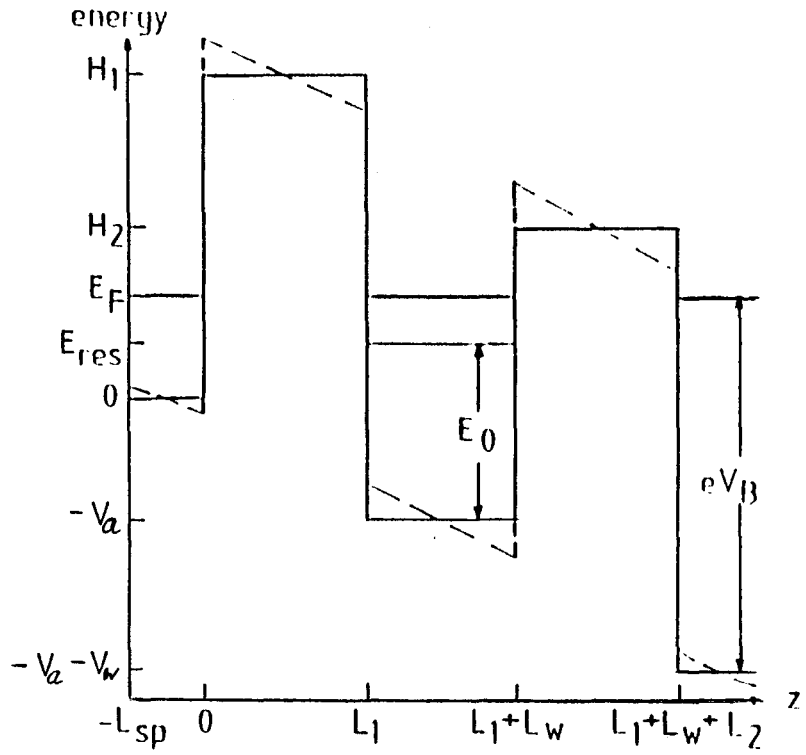

Figure 1 The potential picture of a typical potential structure under bias voltage.

As is shown the potential structure is one-dimensional and the two AlGaAs layers can be regarded as <u>barriers</u> whereas the GaAs layer sandwiched between the barriers behaves like a potential well. As is known from quantum mechanics electrons can tunnel through barriers with a certain transmission probability. Because there is a well with an energy level, electrons with the resonance energy will tunnel resonantly through the structure, which means that their transmission probability is close to one.

The operation of the DBRT is based on the tunability of the resonance energy with respect to the Fermi-sea in the emitter: increasing the applied voltage brings the resonance level first into, then out of the Fermi window. When the current-voltage characteristic of a DBRT is measured, a region of negative differential resistance (NDR) is found, sometimes accompanied by an interval of bistability. Figure 2 shows the current-voltage characteristic of an asymmetric structure (the second barrier is more wide than the second barrier).

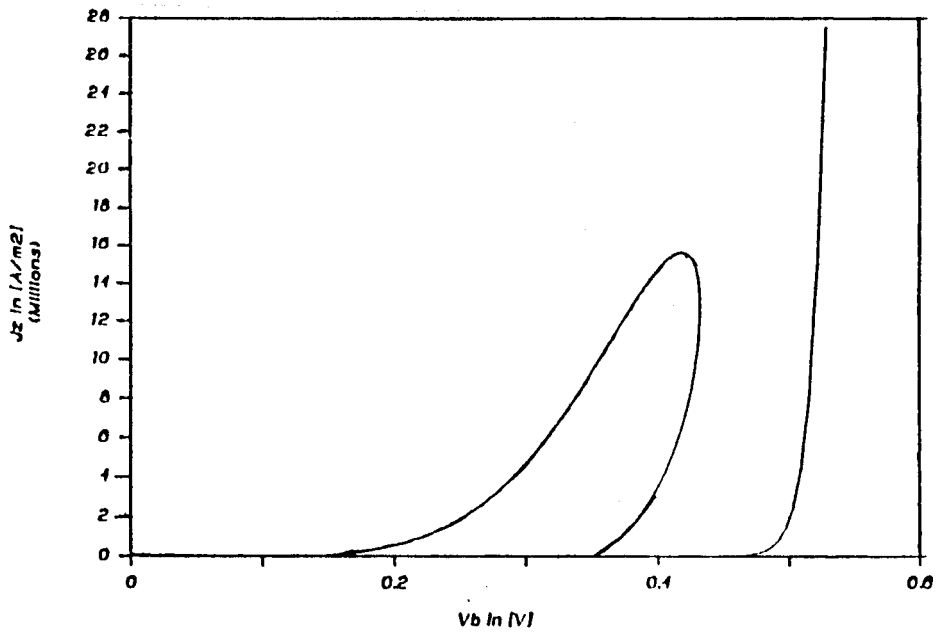

Figure 2 The current voltage characteristic of an asymmetric DBRT structure, at T = 4.2 K, calculated with the model of Noteborn and Joosten [3].

The idea that a DBRT structure can be used as a ultrafast switch is based on the fact that, dependent on the history of the structure (voltage from high to low or vice versa), another current exists. Based on the ultrafast behavior of the DBRT structure, the idea arose that it could be used as a sensor or a laser in the 400 Gigahertz region.

In recent years a lot of experimental work on DBRT structures has been carried out, varying from measuring the I-V curves, determining the dwell times of electrons in the well and magnetic field dependence of the properties of the structure.

Concerning the description of the DBRT, two principal approaches have been put forward. In the sequential approach, advocated by Sheard and Toombs [5], and Eaves [4], among others, electrons tunnel resonantly into the well and loose their phase by thermalization, thus forming an electron gas in the well, that is independent of the emitter equilibrium. A resonance level is borrowed from wave mechanics, whereas transmission probabilities are calculated with a Fermi's Golden Rule type of argument. Hence, a sequential "theory" is hybrid by nature.
In the coherent approach, by Noteborn, Joosten and Lenstra [3], wave coherence throughout the complete structure is assumed. Neither elastic nor inelastic scattering [6] is taken into account. The pure Schrödinger theory allows for the calculation of both resonance level and transmission and reflection coefficients. The I-V characteristics calculated with this approach show NDR and intrinsic bistability. This model describes the truly resonant behavior of the DBRT.

The intrinsic bistability in the I-V characteristics of Double Barrier Structures is in both models closely related to the charge build-up in the well. A magnetic field across the structure appears to be an ideal instrument to probe this charging. In fact the application of a magnetic field is a source of information quite generally. There are two basic geometries, the magnetic field parallel to the current and perpendicular to the current.

$\underline{B} \parallel \underline{J}$ geometry.

The parallel field does not affect the tunneling motion of the electrons but quantizes the lateral motion in all layers. The current shows Shubnikov - de Haas like oscillations with two fundamental periods. Both the sequential- [7] and the coherent- tunneling [8] model are able to

explain these oscillations by relating them to the charge in the emitter and the well: changing the field strength at fixed bias means shifting the Landau levels with respect to the Fermi energy. The resulting oscillations in charge and current density are periodic in 1/B, the periodicity containing the information about the charge distribution [8].

$\underline{B} \perp \underline{J}$ geometry.

In the case of a perpendicular field, the magnetic field does affect the tunneling motion of the electrons. So called skipping orbits arise, which can be compared to the edge current in the Quantum-Hall regime.

This report deals about this geometry and uses the model of Noteborn and Joosten [3] to describe the current and charge in the well as a function of the magnetic field and an applied bias voltage.
In the first chapter we will briefly describe the model of Noteborn and Joosten, based on wave coherence and selfconsistent calculation of charge in the well.
In the second chapter we will consider the changes a transverse magnetic field imposes on Schrödingers equation. The tunnel equation remains one-dimensional but is complicated by the fact that it is not only dependent on the momentum in the z-direction, but also on the momentum in the y-direction. It will appear that the description in Landau levels is not valid whenever there are interfaces present. To calculate the wave function throughout the structure we need boundary conditions that also are dependent on the magnetic field.
In the third chapter we discuss the additional approximations we make with respect to the magnetic field which enable us to make predictions about the current as a function of B and the applied bias voltage.
In the fourth chapter the results are presented. The differences between the results and the predictions of chapter 3 as well as the approximations we made with respect to the magnetic field will be discussed in the last chapter. We will see that charge build up in the well grows dramatically with the magnetic field up to a certain value of the magnetic field, which we call the killing field.

In three Appendices some additional information can be found on the exact solutions of the Schrödinger equation with a transverse magnetic field (Appendix A), the transfer matrix method we used to calculate the wave function throughout the structure (Appendix B) and an extensive calculation of the electron density in the well (Appendix C).

A publication, that contains the basics of this report is in progress.

1. RESONANT TUNNELING IN THE ZERO-FIELD CASE.

In this chapter we give a thorough outline of the model recently presented by Noteborn *et al.* [3]. The main goal of this model is to elucidate the physics of the DBRT-device as much as possible, starting from two basic principles, namely wave-coherence and selfconsistency. In table 1 the layered structure of the device we consider is shown.

500 GaAs	50 GaAs	2.5 GaAs	5.6 barrier AlGaAs	5.0 well GaAs	5.6 barrier AlGaAs	2.5 GaAs	50 GaAs	1000 GaAs	GaAs substr.
2E18 n	2E16 n	und.	undoped	undoped	undoped	und.	2E16 n	2E18 n	2E18 n

Table 1: The layered structure of the DBRT with indicated doping densities. The thickness of the layers is indicated in nanometers.

Wave-coherence means that the electrons obey an effective mass equation [9] in which electron-electron and electron-phonon interactions are neglected, resulting in the phase of the electrons being a constant of motion. The electrons are only affected by the conduction band minimum E_{c0}, which depends on the direction perpendicular on the layers (the z-direction). Thus the effective mass equation reads, with m the effective mass of GaAs in the Γ-minimum:

$$\frac{1}{2m}\,\underline{p}^2\,\Psi_{\underline{k}}(\underline{r}) + E_{c0}(z)\,\Psi_{\underline{k}}(\underline{r}) = E_{\underline{k}}\,\Psi_{\underline{k}}(\underline{r}) \qquad (1)$$

In Eq.(1), $\underline{p}$ is the momentum operator $-i\hbar\underline{\nabla} + e\underline{A}$, where $\underline{A}$ is the vector potential that is dependent of the magnetic field by $\underline{B} = \mathrm{curl}\underline{A}$. The quantity Ψ is an envelope function which describes the trends of the true electron wave function, but neglects the fast Bloch-oscillations. Eq.(1) is a three dimensional equation, but because the conduction band minimum depends only on the z-direction and we only consider the $\underline{A} = 0$ case in this section, it can be written as a one-dimensional equation.

The value of the conduction band minimum E_{c0} will be affected by the charge densities in the structure via Poisson's law (band bending [10]). Thus the band minimum is dependent on the envelope functions by:

$$\nabla^2 E_{c0}(\underline{r}) = - \frac{e^2}{\varepsilon_0 \varepsilon_r} n(\underline{r}) \quad \text{and} \quad n(\underline{r}) = \sum_{\underline{k}} |\Psi_{\underline{k}}(\underline{r})|^2 f_{FD}(E(\underline{k})) \tag{2}$$

So:

$$\nabla^2 E_{c0}(\underline{r}) = - \frac{e^2}{\varepsilon_0 \varepsilon_r} \sum_{\underline{k}} |\Psi_{\underline{k}}(\underline{r})|^2 f_{FD}(E(\underline{k})) \tag{3}$$

In Eq.(3) f_{FD} is the Fermi-Dirac distribution function. When Eq.(1) & (3) are solved simultaneously, the solution is called "self-consistent".

The doped layers on either sides of the five intrinsic layers serve as reservoirs between which conduction is possible. This concept of conduction between reservoirs was introduced by Landauer and Büttiker [11], [12].

One of the aimed features of our model is simplicity, so we make the following assumptions:

We only consider resonant tunneling and neglect all non-resonant contributions. As a consequence, we can neglect contributions to charge and current from electrons out of the reservoir on the right hand side of the structure (where the potential energy is lowest, when a voltage is applied). In the voltage interval of the resonant current, the electrons in this reservoir have energies much smaller than the resonance energy and do not contribute to the current or charge densities in the well. A necessary condition for this neglect is that in the unbiased structure the resonant level is well above the Fermi level.

Also, in our model the Fermi-level is not constant as it would be in a metal, but depends on the applied bias voltage. This could be termed a "pure-semiconductor" picture. Consequently, no doping dependence is found in our E_F.

Further, in order to calculate the current, we consider the charge densities at two sites: in the emitter and in the well. The charge density in the well is by itself two-dimensional. The three dimensional charge

density in the left reservoir is in the doped regions compensated by the donor atoms. Only in the undoped left spacer a net space charge results, that, in the thin spacer layer, is effectively a sheet density. Via Poisson's equation these two "sheet"-densities cause two kinks in the potential energy.

So, an applied bias voltage increases the Fermi-energy, which changes the sheet-densities, that affect the conduction band minima. Eq.(4) denotes the interdependence of the Fermi-energy and the applied bias voltage:

$$V_b = E_F + V_a(E_F) + V_w(E_F) \tag{4}$$

In Eq. (4) V_b is the applied bias over the five intrinsic layers, E_F the freely tunable Fermi-energy in eV, V_a the potential energy drop over the first barrier and the first half of the well, caused by charge accumulation in the left spacer and V_w the potential energy drop over the second half of the well and the second barrier, caused by charge accumulation in the left spacer and the well (see Fig.1). V_a and V_w depend on E_F because the charge densities which cause the kinks depend on E_F. So, Eq.(4) expresses the dependence of the Fermi-energy, to be used in Eq.(3), on the applied bias voltage.

We will now look at the effective-mass-equation (1) with more detail. The doped regions serve as reservoirs from which an electron with wave number $\underline{k}$ can tunnel coherently through the structure. In the reservoirs the envelope functions are plane waves, that interact with the potential structure of the DBRT. The whole device can be characterized by a reflection- and a transmission- coefficient. These coefficients and the envelope function through the whole structure are calculated in the transfer matrix approach (TMA) [13].

At each position where there is a discontinuity in the scalar potential ϕ or the vector potential $\underline{A}$, i.e. at each interface, we have to link the two solutions of the Schrödinger equation. This is done by demanding conservation of probability and probability current, which yields the boundary conditions that enable us to compose an envelope function through the structure. In the zero magnetic field case these boundary conditions are continuity of wave function and continuity of its gradient. In the

next section we will see that a discontinuity in the vector potential changes these boundary conditions.

When the electronic potential is approximated by a piece-wise constant potential, the solutions of (1) are simple plane waves. Any potential picture can be regarded as a series of (infinitely) small regions with constant potential. In our model we choose only three regions, namely the two barriers and the well. It can be shown, that by this approximation no essential changes are introduced in the current-voltage characteristics of a resonant tunneling structure [14]. Figure 1 shows the effective potential electron energy picture which is obtained with this assumption.

The resonance shows up as a sharp peak in the transmission coefficient as a function of the tunnel momentum. Considering resonant tunneling only, amounts to approximating this sharp peak by a δ-function.

With the results of TMA the electron density at position z in the structure is calculated:

$$n_3(z) = g_s \sum_{k_x} \sum_{k_y} \sum_{k_z} |\Psi(\underline{r},\underline{k})|^2 f_{FD}(E(\underline{k})) \tag{5}$$

In Eq. (5), $\underline{k}$ is the wave vector, $|\Psi(\underline{r},\underline{k})|$ the appropriately normalized wave function and $f_{FD}(E(\underline{k}))$ the Fermi-Dirac distribution. It states that the 3D electron density at position z is determined as follows: calculate for all combinations of k_x, k_y, k_z the value of $|\Psi(\underline{r},\underline{k})|^2$, multiply each of them with their occupation number and add them. All electrons originate from the reservoir on the left of the structure, where they are described by plane waves. These plane waves are subject to periodic boundary conditions:

$$\Delta k_x = \frac{2\pi}{L_x} \qquad \Delta k_y = \frac{2\pi}{L_y} \qquad \Delta k_z = \frac{2\pi}{L_z} \tag{6}$$

When the lengths $L_{x,y,z}$ are large enough we can change the summations in Eq.(5) into integrals. The electron density in the left spacer is analytically calculated by transforming the three integrals into one integral over the energy and the result is:

$$\sigma_a = g_s L_{sp} N_c \mathfrak{F}_{1/2}(\beta E_F) \qquad \text{with} \qquad \beta = 1/k_B T \quad N_c = \left(\frac{m}{2\pi\hbar^2\beta} \right)^{3/2} \tag{7}$$

In Eq.(7) L_{sp} is the left spacer length, N_c is the effective number of states per unit volume in the conduction band, $\mathfrak{F}_{1/2}$ is a Fermi-Dirac integral of order 1/2 [8], k_B is Boltzmann's factor and E_F is the Fermi-energy. As the electron density in the well is concerned, the integrals over k_x and k_y can be performed analytically, whereas the integral over k_z is quite simple when the non-resonant current is neglected by means of modeling the energy dependence of the transmission coefficient as a delta function of the energy: $T(E) \sim \delta(E-E_{res})$. This integral is thoroughly described in Appendix 3, which yields that the two dimensional electron density in the well can be written as:

$$\sigma_w = g_s N_c^{2/3} \mathfrak{F}_0(\beta(E_F - E_{res})) \frac{(1-R_1)(1+R_2)}{2(1-R_1R_2)} \tag{8}$$

In Eq.(6), R_i is the reflection coefficient of the i^{th} barrier, E_{res} the resonance energy measured from the conduction band minimum of the left spacer and $\mathfrak{F}_0$ a Fermi-Dirac-integral of 0^{th} order [15].

In the same way the current density J_z can be determined. Since J_z is independent of z, we can evaluate it at any position. We take for this position the right hand side of the second barrier. With Eq.(5) we can calculate what charge density is present at that position. Note that in our model, no charge density is considered at that position; we assume that at that position no charge accumulates but will flow immediately into the right reservoir. The result can be expressed in the charge density in the well and the reflection coefficient of the second barrier:

$$J_z = e \frac{\sigma_w}{L_w} \frac{1-R_2}{1+R_2} \sqrt{2(E_{res} + V_a)/m} \tag{9}$$

Equations (4) and (9), together with (7) and (8), are a parametric

description of the selfconsistently determined I-V characteristic, the Fermi-energy E_F being the parameter. When two current density values are possible at the same V_b, we have bistability. Because the set of equations forms an iterative problem the help of a computer is needed. Figure 3 shows some examples of numerically solving Schrödinger's and Poisson's equation.

In the next chapter we will see how a transverse magnetic field affects the model and its results.

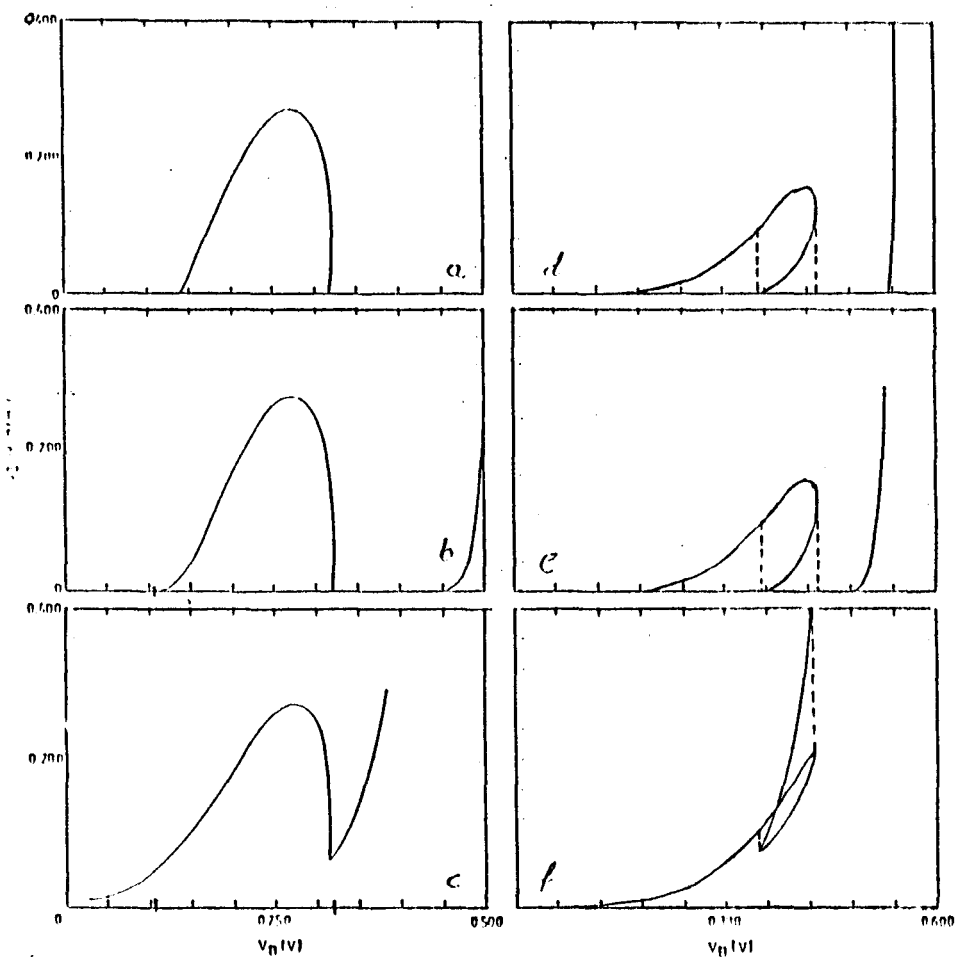

Figure 3 The current voltage characteristics resulting from numerically solving Poisson's and Schrödinger's equation simultaneously, for the symmetric sample (L_2=L_1), at T = 4.2 K (a), at T = 77 K (b), and at 300 K (c); and for the asymmetric sample (L_2>L_1), at T = 4.2 K (d), at T = 77 K (e), and at T = 300 K (f).

2. TRANSVERSE MAGNETIC FIELD; THEORY.

2.1 Schrödinger's equation in a transverse magnetic field.

In this chapter we will first discuss the changes a transverse magnetic field imposes on Schrödinger's equation. Let us consider Schrödinger's equation when no bias voltage is applied and no layered structure is present, so E_{c0} in Eq.(1) is constant. Let the z-axis be perpendicular to the layers and the magnetic field $\underline{B}$ constant in the x-direction: $\underline{B}$ = (B,0,0). As is well known from classical electrodynamics, the Lorentz force $-e\underline{v} \times \underline{B}$ causes an electron to describe a cyclotron orbit with cyclotron frequency $\omega_c = eB/m$, with m the appropriate mass of the electron.
In quantum mechanics the description in cyclotron orbits is not so obvious anymore. This can be related to the fact that the magnetic field $\underline{B}$ has no explicit appearance in the Hamiltonian. Instead, the vector potential $\underline{A}$ appears in the Hamiltonian:

$$H_{op} = \frac{1}{2m}\,\underline{p}_{op}^{2} - e\phi, \text{ with } \underline{p}_{op} = \frac{\hbar}{i}\,\underline{\nabla} + e\underline{A} \tag{10}$$

Thus the current operator also depends on $\underline{A}$ and ϕ. The magnetic field $\underline{B}$ and the electric field $\underline{E}$ are related to the vector potential $\underline{A}$ and the scalar potential ϕ by $\underline{B} = \text{curl}\underline{A}$ and $\underline{E} = -\frac{\partial}{\partial t}\underline{A} - \underline{\nabla}\phi$. This means that there is an infinite number of $(\underline{A},\phi)$ combinations that yield the same $\underline{B}$ and $\underline{E}$. When the gauge-transformation $\underline{A}' = \underline{A} + \underline{\nabla}f$ and $\phi' = \phi - \frac{df}{dt}$ is performed, with f a non-singular function, $\underline{A}'$ and ϕ' yield the same $\underline{B}$ and $\underline{E}$. The charge density ρ and the current density $\underline{J}$ are not influenced by this transformation because it is canonical (gauge-invariance), so we can choose a gauge to our own convenience [16].
In our example of a non-layered region without bias voltage and with constant E_{c0} the effective mass equation, with $\underline{A}$ = (0,-Bz,0), reads:

$$-\frac{\hbar^2}{2m}\nabla^2\Psi + i\hbar\omega_c\, z\,\frac{\partial\Psi}{\partial y} + \tfrac{1}{2}m\omega_c^2\, z^2\Psi = (E - E_{c0})\Psi \tag{11}$$

When we make the Ansatz $\Psi(x,y,z) = \exp(ik_x x)\cdot\exp(ik_y y)\cdot F(z)$, Eq.(11) can be written as:

$$-\frac{\hbar^2}{2m}\frac{d^2}{dz^2}F(z) + \left(\frac{1}{2}m\omega_c z - \hbar k_y\right)\omega_c z F(z) = E_3 F(z) \qquad (12)$$

where $E_3 = E - E_{c0} - \hbar^2k_x^2/2m - \hbar^2k_y^2/2m$. Solutions of Eq.(12) not only depend on E_3, but also on k_y, i.e. an "eigen" function F(z) will have two parameters: k_y and E_3. Note that putting B = 0 ($\omega_c = 0$) in Eq.(12) removes the k_y dependent term: In the zero-field case, true separation of variables is possible. In the $B \neq 0$ case, however, it is the magnetic field that introduces a dependence of tunnel function F(z) on the lateral momentum k_y. Consequently, we will have to consider each k_y separately.

2.2 Solutions

Equation (12) can be considered an ordinary Schrödinger problem with a quadratic potential. The harmonic oscillator problem is of the same kind, so we expect the solutions of Eq.(12) to be equivalent to the ones of the harmonic oscillator. In order to write Eq.(12) in a more recognizable form we make it dimensionless by substituting, with ℓ_m a magnetic length $(\hbar/eB)^{1/2}$, $\zeta = z/\ell_m - k_y\ell_m$ and $E' = E - E_{c0} - \hbar^2k_x^2/2m$:

$$\frac{d^2}{d\zeta^2}F(\zeta) + \left(\frac{2E'}{\hbar\omega_c} - \zeta^2\right)F(\zeta) = 0$$

This is the equation of the harmonic oscillator problem [35], [36]. The solutions of a differential equation depend in general on the boundary condition(s). In the harmonic oscillator problem, the boundary condition is the requirement of normalizability of the wavefunctions (if they are not, they do not have physical meaning). This boundary condition leads to the well known quantization of energies. When the oscillator frequency is the cyclotron frequency, these energy-levels are called Landau-levels [37].

Note that the existence of these Landau levels solely depends on the demand of normalizability. If Eq.(12) is to be solved for a layered structure and/or a confined magnetic field, this demand may no longer lead to Landau levels in the strict sense of quantization as in the harmonic oscillator problem. We will illustrate this by looking for the complete set of solutions of Eq.(12). We again start with Eq.(12) and make it dimensionless in a similar way; by substituting $\zeta = \sqrt{2}(z/\ell_m - k_y \ell_m)$ and $\alpha^2 = E_3/\hbar\omega_c$ and $\lambda^2 = \frac{1}{4}$ we get:

$$\frac{d^2}{d\zeta^2} F(\zeta) + (\alpha^2 - \lambda^2\zeta^2)F(\zeta) = 0 \qquad (13)$$

Equation (13) is known as **Weber's** *differential equation* [36]. It is a special form of the *Hypergeometric Differential Equation,* solutions of which are known as hypergeometric functions [17]. In the textbooks, several representations are encountered. The solutions of Eq.(13) can be expressed in Kummer functions [17], Parabolic cylinder functions [18], [19] and confluent hypergeometric functions [17]. In this report we will use the representation in parabolic cylinder functions. In Appendix A some properties, expansions and recursion relations are given. By rewriting Eq.(13) with $\nu + \frac{1}{2} = \alpha^2$, we get:

$$\frac{d^2}{d\zeta^2} F(\zeta) + (\nu + \tfrac{1}{2} - \tfrac{1}{4}\zeta^2)\, F(\zeta) = 0 \qquad \underline{\nu \in \mathbb{R}} \qquad (14)$$

From Eq.(14) we see that if $D_\nu(\zeta)$ is a solution, so are:

$$D_\nu(-\zeta), \qquad D_{-\nu-1}(i\zeta), \qquad D_{-\nu-1}(-i\zeta) \qquad (15)$$

From these, we can choose $D_\nu(\zeta)$ and $D_{-\nu-1}(i\zeta)$ as a set of linearly independent solutions to the second order differential equation (14).

If ν is restricted to positive integer values, the solutions of Eq.(14) can be expressed in terms of Hermite polynomials $H_n(\zeta)$:

$$D_n(\zeta) = \sqrt{2}\exp(-\frac{\zeta^2}{4})\, H_n(\sqrt{2}\zeta) \qquad n \in \{0,1,2,\ldots\} \tag{16}$$

which go to zero for $|\zeta| \longrightarrow \infty$, and are therefore acceptable wavefunctions for the harmonic oscillator. The accompanying $D_{-n-1}(i\zeta)$, however, are unbounded on the interval $-\infty < \zeta < \infty$, and, although a regular solution of Eq.(14), are not acceptable as wavefunctions, and are therefore rarely encountered in textbooks.

If ν is nonintegral, both $D_\nu(\zeta)$ and $D_{-\nu-1}(i\zeta)$ are unbounded on one side (see Fig.4).

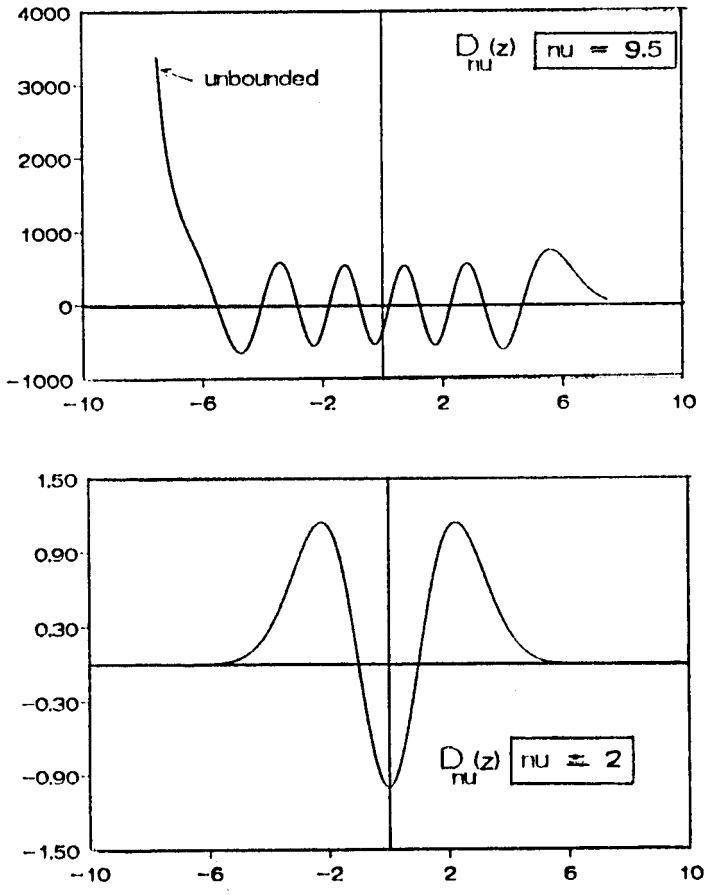

Figure 4. A parabolic cylinder function with ν noninteger, which is unbounded in $\zeta = -\infty$; and a parabolic cylinder function with ν a positive integer, which is bounded.

The fact that they are unbounded does not mean that they are not useful as wave functions. Only in cases where there are no boundaries in ζ, like in the harmonic oscillator problem, they can not be used.
This means that the Landau levels will be disturbed whenever an interface is present, because that allows other energies too (see e.g. [20], [21]).
In Appendix A1 a presentation of the parabolic cylinder functions is given with regard to their use in the transfer matrix formalism.

2.3 Boundary Conditions

When the magnetic field stretches out to infinity the electrons can only be described by bound states (Landau levels), so no current is possible. Therefore it is necessary to confine the magnetic field to some region. There are two gauge choices to describe this (see Fig.5). In the first the vector potential is chosen continuous, which introduces a region on the z-axis where $\underline{B} = 0$ but $\underline{A} \neq 0$. In the second, we make $\underline{A} = 0$ whenever $\underline{B} = 0$ which introduces at least one z at which $\underline{A}$ is discontinuous.

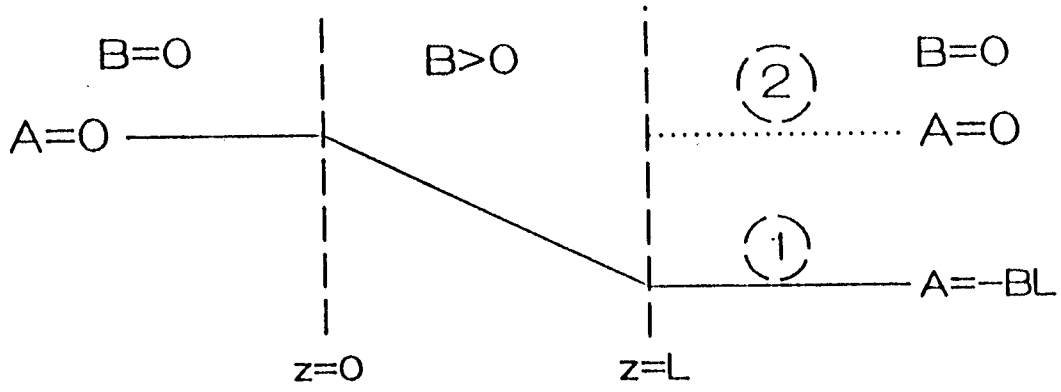

Figure 5 The two choices of gauges. Number two leaves the Schrödinger equation in the right reservoir unharmed, but has a discontinuity in the vectorpotential.

When the first option is chosen, which does not imply any discontinuities in the vector potential, the description of electrons in the right reservoir is somewhat complicated. Because in the right reservoir there now is a nonzero vector potential, the wavefunction contains a phase factor, which is dependent of A. This seems unnatural, but we can not

change physics. However, if we choose the second option, this problem is avoided. Because there is now a discontinuity in the vector potential the boundary conditions have to be reviewed.

In Schrödinger's theory the meaning of charge density ρ and current density $\underline{J}$ is unambiguous, that is independent of gauge. We will therefore base our boundary conditions on these two quantities. ρ and $\underline{J}$ are related to the wave function of an electron in the following way:

$$\rho(\underline{r}) = e\,|\Psi(\underline{r})|^2 \tag{17a}$$

$$\underline{J}(\underline{r}) = \frac{e}{2m}\left\{\Psi^*(\underline{r})\underline{p}_{op}\Psi(\underline{r}) + \text{c.c.}\right\} \tag{17b}$$

In Eq.(17b) $\underline{p}_{op}$ is the canonical momentum operator $-i\hbar\underline{\nabla} + e\underline{A}$. At an interface the ρ and $\underline{J}$ must be both continuous, because we work in the time-independent case, so the boundary conditions are continuity of $\Psi(\underline{r})$ and continuity of $\underline{p}_{op}\Psi(\underline{r})$.

Consider an interface at $z = z_0$. The wave functions on either sides of the interface are given by (with α a constant):

$$\Psi_\ell(x,y,z) = \exp(ik_{x\ell}x)\exp(i(k_{y\ell}+\alpha)y)F_{k_{y\ell}}(z) \qquad z < z_0 \tag{18a}$$

$$\Psi_r(x,y,z) = \exp(ik_{xr}x)\exp(ik_{yr}y)F_{k_{yr}}(z) \qquad z > z_0 \tag{18b}$$

The four equations then read:

$$\exp(ik_{x\ell}x)\exp(i(k_{y\ell}+\alpha)y)F_{k_{y\ell}}(z_0) = \exp(ik_{xr}x)\exp(ik_{yr}y)F_{k_{yr}}(z_0) \tag{19a}$$

$$\left(-i\hbar\frac{\partial}{\partial x} + eA_{\ell x}\right)\Psi_\ell(x,y,z)\Big|_{z=z_0} = \left(-i\hbar\frac{\partial}{\partial x} + eA_{rx}\right)\Psi_r(x,y,z)\Big|_{z=z_0} \tag{19b}$$

$$\left(-i\hbar\frac{\partial}{\partial y} + eA_{\ell y}\right)\Psi_\ell(x,y,z)\Big|_{z=z_0} = \left(-i\hbar\frac{\partial}{\partial y} + eA_{ry}\right)\Psi_r(x,y,z)\Big|_{z=z_0} \tag{19c}$$

$$\left(-i\hbar\frac{\partial}{\partial z} + eA_{\ell z}\right)\Psi_\ell(x,y,z)\Big|_{z=z_0} = \left(-i\hbar\frac{\partial}{\partial z} + eA_{rz}\right)\Psi_r(x,y,z)\Big|_{z=z_0} \tag{19d}$$

In the $\underline{A}$ = (0,0,0) case, these reduce to:

$$k_{x\ell} = k_{xr} \quad k_{y\ell} = k_{yr} \quad \alpha=0 \qquad \frac{d}{dz} \ln F_{\ell}(z_0) = \frac{d}{dz} \ln F_{r}(z_0) \tag{19f}$$

If, however, $\underline{A}$ = (0,-Bz,0), we find the second condition changed into:

$$k_{y\ell} = k_{yr} + \frac{e}{\hbar} (B_{\ell}-B_{r})z_0 \tag{20a}$$

If we set $\alpha = \frac{e}{\hbar} (B_{r}-B_{\ell})z_0$, the y-dependent part of the wavefunction is continuous. Thus, the discontinuity in A yields a discontinuity in k_y.

So, not only because of Schrödinger's equation but also because of the boundary conditions it is necessary to consider each k_y separately. In the next chapter we will describe the changes a transverse magnetic field imposes on our model, and discuss the approximations we made with respect to the magnetic field.

3. MODEL APPROXIMATIONS AND PREDICTIONS

3.1 Model approximations

The model we use for the DBRT-structure under bias and a transverse magnetic field has its origin in the model for the zero field case described in the first chapter. In this section we will discuss the approximations we make with respect to the magnetic field, and their implications for the electron density in the well and the resonant current through the structure.

In the previous chapter the 1D-Schrödinger equation for magneto tunneling was derived (Eq.(12)). It contains a potential energy term that depends on the lateral momentum k_y. The total potential for an electron tunneling through a DBRT structure under a bias voltage and with a transverse magnetic field reads:

$$U_{k_y}(z) = \frac{\hbar^2}{2m}\left(\frac{eBz}{\hbar} - k_y\right)^2 + E_{c0}(z) \qquad (21)$$

where $E_{c0}(z)$ describes the conduction band minimum as a function of z. In the model described in chapter 1, we saw that the conduction band minimum is modeled as a piece-wise constant one in order to work with plane waves.

Confinement

We can not let the magnetic field stretch out infinitely, because then all electrons would be in bound states and no current would be possible. Therefore we must confine the magnetic field to a finite region. For reasons of simplicity we choose this region only to include the two barriers and the well. This does not yield any extra interfaces, so it does not complicate calculations with respect to the transfer matrix formalism. Experimentally this may be unrealistic to a certain extent, but the qualitative results will not change much because of this.

Theoretically, a partial justification may be found in the phase-mixing, coherence destroying processes active in the reservoir layers, that are to be hold responsible for a diminished influence of the magnetic field in these parts of the structure.
A further adhortation is derived from the fact that this choice of confinement is not unusual in literature: Brey, Platero and Tejedor [23], [24], as well as Büttiker [25] and Ancilotto [26] also confine the magnetic field to the two barriers and the well. Experiments will have to determine what region should be taken for the magnetic field, but we will come to that in the discussion.

Piece wise constant potential energy

From the above discussion it would seem natural to do TMA calculations with parabolic cylinder functions for the central part of the structure, and plane waves for the reservoir layers, linked together at the two barriers according to the boundary conditions of the previous section (Eq.(20a)). However, computational difficulties in finding a stable algorithm for the parabolic cylinder functions $D_\nu(\zeta)$ for all relevant ν and ζ, see Appendix A, have forced us to choose a slightly different approach.
In analogy to the electrostatic potential, the quadratic "magnetic potential" is modeled as a piece-wise constant function. We will use the simplest (i.e. crudest) intervalling possible, considering only three regions.
As a consequence, we can work with plane waves also in the structure. The mean value of the potential energy in a region stretching from $z=z_0$ to $z=z_e$:

$$\overline{U}_{k_y}(z_0,z_e,B) = \frac{1}{6}m\omega_c^2\left((z_e+z_0)^2 - z_e z_0\right) - \frac{1}{2}\hbar\omega_c k_y(z_0+z_e) + \frac{\hbar^2}{2m}k_y^2 \qquad (22)$$

is used as the constant potential energy value on that interval.
Before we will make some predictions about the current with the help of this modeling of the potential energy, we describe the calculation of both

the current density and the electron density in the well, because their calculation is altered by the magnetic field.

Electron density in the well

In the above we showed that a transverse magnetic field, represented by the gauge $\underline{A}$ = (0,-Bz,0), forces us to consider the wavefunction for each k_y separately. This means also that in calculating the electron densities in front of the first barrier and in the well we cannot perform the summation over k_y separately from the one over k_z (See Eq.(5)).
In this case we can only perform the summation over k_x analytically, which results in a Fermi-Dirac integral of order -1/2 depending on the remaining wave numbers k_y and k_z. Of the numerical summations over k_y and k_z, we first perform the one over k_z, so that we can express the charge density as a sum over contributions labeled by k_y:

$$n_3(z) = \frac{g_s}{8\pi^3}\left(\frac{m\pi}{2\hbar^2\beta}\right)^{1/2}\int_{-\infty}^{\infty}dk_y\int_{-\infty}^{\infty}dk_z\left|F(z;k_y;k_z)\right|^2\,\mathfrak{F}_{-1/2}\left(\frac{E_F-E(k_y,k_z)}{k_BT}\right) \qquad (23)$$

Of course, the charge density in the left spacer is easier to calculate than Eq.(23) implies, as was shown in the section about resonant tunneling without magnetic field. Thus we have to concentrate on determining the charge density in the well. For the value of $|F|^2$ in Eq.(23) we take the average value of the wave function inside the well. In chapter 1 we saw that considering only the resonant contributions to charge and current simplifies calculations considerably (δ-function approximation of transmission [3]). With the transverse magnetic field we can maintain this approximation but now for each k_y separately. The expression for the charge density in the well thus becomes similar to Eq.(8), be it that it is dependent of k_y. See Appendix 3 for a detailed description of the calculation of the electron density in the well.

Current density

Analogously, the current density can be regarded as the sum of k_y contributions:

$$J_z = \int_{-\infty}^{\infty} dk_y \; j_z(k_y) \tag{24}$$

However, a complication arises here, that has no analog in the zero-field case. Whereas, at B = 0, all resonant electrons that can reach the well, also reach the collector, and thus contribute to the current density, now at $B \neq 0$ we can have electrons with positive kinetic energy in the well but negative kinetic energy in the collector. Hence, these electrons still contribute to the the electron density in the well but no longer to J. How to distinguish between resonant- (contributing to <u>both</u> charge and current) and quasi-bound- electrons (contributing only to the charge), is outlined in Appendix B. This typical magnetic field effect will be outlined in the next section.

The modeling of the potential energy as a piece-wise constant one will prove to be a big help in determining whether electrons at given values of V_b and B are allowed to participate in the current. In the next section we will elaborate on this and make some predictions about the current as a function of the applied bias voltage and the transverse magnetic field.

3.2 Prediction of Start- and End- Voltages

In analyzing the voltages at which a current starts or ends, we use the following picture, using the nomenclature of chapter 1 (V_i is the conduction band minimum in the i^{th} region, E_0 is the energy of the level in the well measured from the conduction band minimum in the well):

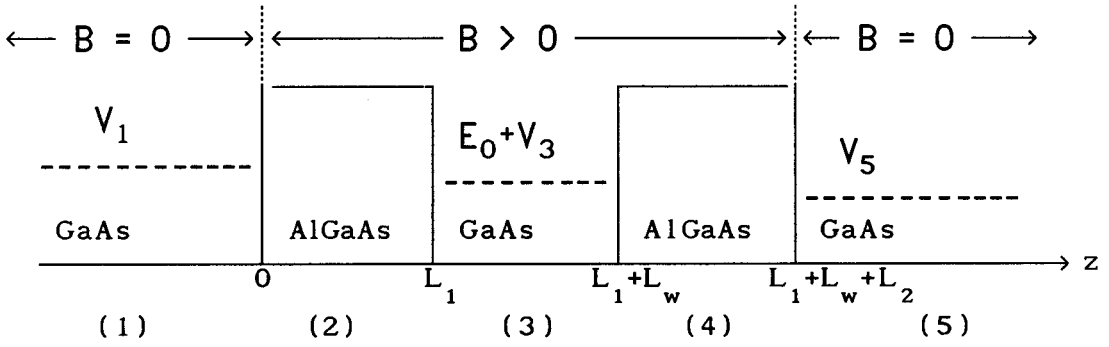

Fig. 6: The three potential energies whose relative positions determine whether an electron can tunnel resonantly in the well and can participate in the resonant current. The zero of the energy scale is the energy of an electron with k_z equals zero and with k_y such that Eq.(22) is zero.

At zero temperature, electrons can only enter the well when E_0+V_3 is in the window of the Fermi sea in the left spacer. In this section, we neglect the very small shift of the resonance level due to biasing and assume the resonance energy E_0, measured from the conduction band minimum of the well, to be constant.

We first discuss the B=0 case because there the value of k_y is not relevant for determining whether a current is possible.

Zero magnetic field

Recall that in the zero field case all electrons that tunnel resonantly into the well participate in the current, because V_5 is always smaller than E_0+V_3 (independent of k_y). A current starts when the resonance channel is in reach of the electrons in the Fermi-sea. The resonance channel lies above the Fermi-sea when V_b equals zero so a current starts when:

$$E_F + V_1 = E_0 + V_3 \tag{25}$$

Note that the Fermi energy as well as V_1 and V_3 are dependent of the applied bias voltage.
Similarly there is a V_b that lifts the Fermi-sea completely above the resonance channel. This happens first when:

$$V_1 = E_0 + V_3 \tag{26}$$

We now solve Eq.(25) and (26). Since in both cases there is no charge present in the well, so V_3 is simply proportional to V_1, this yields for Eq.(25):

$$E_F + V_a + V_w = E_0 + V_w \tag{27}$$

Substituting that $V_a = \frac{L_w/2 + L_1}{L_1 + L_w + L_2} A E_F^{3/2}$,

$$A = (L_1+L_w+L_2)L_{sp}\, g_s \frac{1}{6} \pi^{-2}(2m/\hbar^2)^{3/2} \frac{e^2}{\varepsilon_0 \varepsilon_r} \tag{28}$$

yields an equation for $E_{F,start}$:

$$E_{F,start} + \frac{L_w/2 + L_1}{L_1 + L_w + L_2} A E_{F,start}^{3/2} = E_0 \tag{29}$$

that is related to $V_{b,start}$ via $V_{b,start} = E_{F,start} + A E_{F,start}^{3/2}$.

Solving Eq.(29) with Newton's method yields for $V_{b,start}$ about 0.13 volts, in agreement with the I-V curves of Fig.3. In the same way, Equation (26) gives the voltage $V_{b,end}$ at which the resonant current disappears:

$$\frac{L_w/2 + L_1}{L_1 + L_w + L_2} AE_F^{3/2} = E_0 \quad \Leftrightarrow \quad V_{b,end} \approx 0.31 \text{ volts} \tag{30}$$

Non-zero field

As was indicated in the previous chapter, a transverse magnetic field complicates the calculation of the special voltages, because of the dependence on k_y of the potential.
We first write down the expressions for the three relevant potential energies in a symmetric DBRT structure (L_1=L_2):

$$V_1(k_y,B) = \frac{\hbar^2}{2m}k_y^2 + V_a + V_w \tag{31}$$

$$V_3(k_y,B) = \overline{U}_{k_y}(L_1, L_1+L_w, B) + V_w \tag{32}$$

$$V_5(k_y,B) = \frac{\hbar^2}{2m}k_y^2 - \hbar\omega_c k_y(2L_1+L_w) + \frac{1}{2}m\omega_c^2(2L_1+L_w)^2 \tag{33}$$

The k_y-contribution to the resonant charge build-up in the well will be nonzero, only when:

$$V_1(k_y,B) < E_0 + V_3(k_y,B) < V_1(k_y,B) + E_F - \frac{\hbar^2}{2m}k_y^2 \tag{34a}$$

For k_y to also contribute to the current, a further condition must be satisfied:

$$E_0 + V_3(k_y,B) > V_5(k_y,B) \tag{34b}$$

At a fixed bias voltage, conditions (34a) and (34b) may be satisfied for some k_y and violated for other k_y. We now examine systematically

conditions (34a) and (34b).

First we examine the entering of the resonance channel in the Fermi-sea:

$$V_a + V_w + E_F \geq \overline{U}_{k_y}(L_1, L_1+L_w, B) + V_w + E_0 \tag{35}$$

Again we assume no charge in the well (at smaller voltages the resonance channel is out of the range of the Fermi-sea) so we can use Eq.(28):

$$E_F + \tfrac{1}{2}AE_F^{3/2} \geq E_0 + \tfrac{1}{2}m\omega_c^2(L_1^2 + L_1L_w + \tfrac{1}{3}L_w^2) - \tfrac{1}{2}\hbar\omega_c k_y(2L_1 + L_w) + \frac{\hbar^2}{2m}k_y^2 \tag{36}$$

Equation (36) leads to a $V_{b,start}(k_y)$ for all $|k_y| < k_F$. To find the overall $V_{b,start}$ of the I-V curve we have to minimize $V_{b,start}(k_y)$ with respect to k_y. We therefore look for the smallest voltage, i.e. the lowest Fermi energy, which has:

$$\exists k_y \in [-k_F, k_F]:$$

$$E_F + \tfrac{1}{2}AE_F^{3/2} \geq E_0 + \tfrac{1}{2}m\omega_c^2(L_1^2 + L_1L_w + \tfrac{1}{3}L_w^2) - \tfrac{1}{2}\hbar k_y\omega_c(2L_1 + L_w) + \frac{\hbar^2}{2m}k_y^2 \tag{37}$$

The right hand side of (37) is minimal for $k_y = m\omega_c(L_1 + \frac{1}{2}L_w)/\hbar$. When that is greater than k_F, the right hand side of (37) is minimal for $k_y = k_F$. This means that electrons with this k_y are the first ones to tunnel resonantly into the well.

We can thus calculate the bias voltage at which the first electrons enter the well as a function of the magnetic field. The results are shown in Fig.7.

We now look for the lowest voltage at which no electrons can enter the well. The resonance energy then is smaller than the conduction band minimum in the left spacer. We therefore look for the lowest bias voltage, so also the lowest Fermi energy, which has:

$$\forall k_y \in [-k_F, k_F]: \frac{\hbar^2}{2m}k_y^2 + V_a + V_w \geq \overline{U}_{k_y}(L_1, L_1+L_w, B) + V_w + E_0 \tag{39}$$

This can be written as:

$$\forall_{k_y \in [-k_F, k_F]}: \frac{1}{2}AE_F^{3/2} \geq E_0 + \frac{1}{2}m\omega_c^2(L_1^2 + L_1L_w + \frac{1}{3}L_w^2) - \frac{1}{2}\hbar\omega_c k_y(2L_1 + L_w) \quad (40)$$

The right hand side of (40) is maximal when k_y is minimal, so $k_y=-k_F$. This means that the electrons with $k_y=-k_F$ are the last ones that can tunnel resonantly into the well. We solve:

$$\frac{1}{2}AE_F^{3/2} - \frac{1}{2}(2L_1+L_w)\omega_c\sqrt{2mE_F} = E_0 + \frac{1}{2}m\omega_c^2(L_1^2 + L_1L_w + \frac{1}{3}L_w^2) \quad (41)$$

The solutions of Eq.(41), calculated with Newton's method, are shown in Fig.7.

As stated above, it is not sufficient to have V_b between $V_{b,start}$ and $V_{b,end}$, to find a nonzero current. In contrast to the zero-field case, the intervals of current and of charge build-up in the well, do not coincide now. In order to find the subinterval of $(V_{b,start}, V_{b,end})$ where resonant current is possible, we consider condition (34b) and compare it with the previous solutions.

This third condition is satisfied when the resonance channel lies above the conduction band minimum of the right hand side. We again assume that there is no charge in the well, although this is not very realistic. Calculations will show how the charge in the well, as well as selfconsistency affect the inequalities. We will return to this matter in the discussion. The condition reads:

$$AE_F^{3/2} \geq -2E_0 + m\omega_c^2(3L_1^2 + 3L_1L_w + \frac{2}{3}L_w^2) - \hbar\omega_c k_y(2L_1 + L_w) \quad (42)$$

Condition (42) is hard to be violated for small magnetic fields, but for higher magnetic fields the right hand side will be positive for some k_y and could then be the decisive inequality.

When condition (42) is satisfied for the $V_{b,start}$ we found with Eq.(38), $V_{b,start}$ is the voltage at which the current begins. If (42) is violated for that k_y, the start voltage will be higher than $V_{b,start}$. But when the voltage is higher than $V_{b,start}$, more electrons than the ones with $k_y = k_F$

will enter the well and it is not obvious to tell what electrons are permitted to tunnel through the second barrier and what electrons stay behind in the well, because our assumption of no charge in the well does not hold anymore so we can not use Eq.(28).

When condition (42) is satisfied for the $V_{b,end}$ we found with Eq.(41), $V_{b,end}$ is the voltage above which no current exists. When condition (42) is violated, the end voltage will be smaller than $V_{b,end}$. But then more electrons than the ones with $k_y = -k_F$ will enter the well so Eq.(28) does not hold anymore.

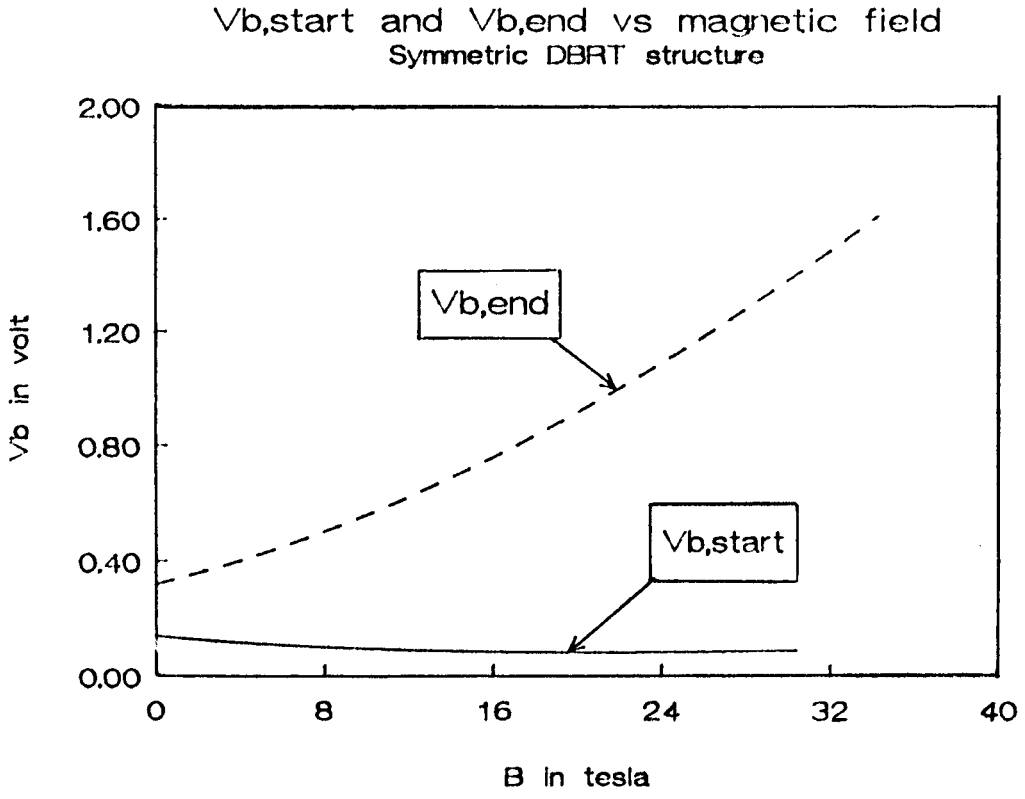

Figure 7, The predicted values of the start- and end- voltages, assuming no charge in the well, for the symmetric DBRT structure. The lines stop when for the electrons that just can enter the well, the resonance channel lies below the conduction band minimum of the right spacer.

As is shown in Fig.7, our analysis is only valid for those magnetic fields where no charge is in the well when the current starts or ends. Only selfconsistent calculations, that take the charge in the well into account, can give a decisive answer about the start and end voltages at larger magnetic fields.

3.3 The Killing Field

Figure 7 raises the question whether the voltage range in which current exists will grow monotonously with the transverse magnetic field, or whether the current will vanish at some value of B. The latter is the case when for all values of the bias voltage the propagation of all electrons is described by a non-current carrying transfer matrix. We again look at the relative positions of the potential energies as shown in Fig.6. When we neglect the charge in the well, we can use Eq.(28). The selfconsistent calculations will show to what extent this condition is satisfied. When the resonance channel has the same potential energy as the conduction band minima of both the left and the right spacer, no electrons can resonantly enter the well, let alone participate in a resonant current. Using Eq.(28), we solve:

$$V_1(k_y,B) = E_0 + V_3(k_y,B) = V_5(k_y,B) \tag{43}$$

This yields:

$$E_0 + V_3 = V_1 \Leftrightarrow AE_F^{3/2} = 2E_0 + m\omega_c^2(L_1^2+L_1L_w+\tfrac{1}{3}L_w^2) - \hbar\omega_c k_y(2L_1+L_w) \tag{44}$$

$$E_0 + V_3 = V_5 \Leftrightarrow AE_F^{3/2} = -2E_0 + m\omega_c^2(3L_1^2+3L_1L_w+\tfrac{2}{3}L_w^2) - \hbar\omega_c k_y(2L_1+L_w) \tag{45}$$

Equation (45) does not allow electrons to enter the well, independent of the bias voltage, as long as the Fermi level does not become higher than the first barrier. Solving Eq.(44) and (45) yields the magnetic field at which for all bias voltages no k_y can enter the well:

$$B = \frac{1}{e}\left(\frac{8mE_0}{L^2 - \frac{1}{3}L_w^2}\right)^{1/2} \tag{46}$$

where $L = L_1+L_w+L_2$ is the total structure length. The term $L_w^2/3$ is due to averaging the potential energy in the well over L_w. If $L_w = L/3$, then in good approximation:

$$B = \frac{(8mE_0)^{1/2}}{eL} \tag{46a}$$

We will call this value of B the *killing field*, because at higher values of B, no resonant current is possible: at bias voltages that allow electrons to enter the well, the resonance channel lies below the conduction band minimum of the right spacer; at bias voltages that allow any present electrons to leave the well into the right spacer, the resonance channel lies below the conduction band minimum of the left spacer so no electrons will be present in the well. For our structure the value of the killing field is about 34.2 T.

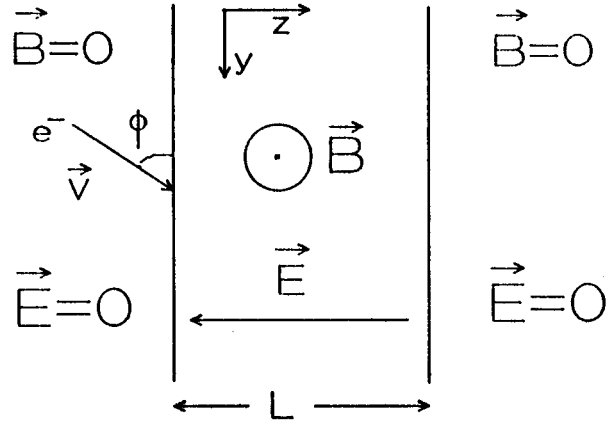

Figure 8 The classical picture of an electron with velocity v, and an angle φ,entering a region with length L, where a transverse magnetic field and an electric field is present.

We will now examine, whether there is such a thing as a killing field in classical electrodynamics. We therefore consider the situation shown in Fig.8. An electron with mass m moving with a velocity v_s in the z-direction in a region where there is neither a magnetic field nor an electric field enters a region where there is a constant transverse magnetic field and a constant accelerating electric field. This region is confined to a length L. In the region z>L again there is no magnetic field nor an electric field. The orientation of the axes is denoted in the figure.

Let us write down the Lorentz force acting on the electron:

$$\underline{F} = m\dot{\underline{v}} = -e\underline{E} - e(\underline{v} \times \underline{B}) = -e\ (0,0,-E) - e\ (0,v_z B,-v_y B) \tag{47}$$

With $\omega_c = eB/m$ the cyclotron frequency, the vector equation Eq.(47) can be written as the following differential equations using $\underline{v} = (v_x,v_y,v_z)$:

$$\dot{v}_x = 0 \qquad v_x(0) = 0 \tag{48a}$$

$$\dot{v}_y = -\omega_c v_z \qquad v_y(0) = v_s \cos\varphi \tag{48b}$$

$$\dot{v}_z = eE/m + \omega_c v_y \qquad v_z(0) = v_s \sin\varphi \tag{48c}$$

Taking the time-derivative of Eq.(48c) yields, together with Eq.(48b):

$$\ddot{v}_z = \omega_c \dot{v}_y = -\omega_c^2 v_z \qquad v_z(0) = v_s \sin\varphi \tag{49}$$

The solution of Eq.(49) is dependent on the starting value v_s:

$$v_z(t) = \alpha \sin(\omega_c t+\theta), \qquad \alpha \sin\theta = v_s \sin\varphi \tag{50}$$

With Eq(50) we get $v_y(t)$ from Eq.(48c):

$$v_y(t) = \alpha \cos(\omega_c t+\theta) - \frac{E}{B} \qquad \alpha \cos\theta - E/B = v_s \cos\varphi \tag{51}$$

It is clear that when both v_s and E equal zero the electron will not enter the region where the transverse magnetic field is present, because then α equals zero. With Eq.(48a), (50) and (51) we solve:

$$\dot{x} = 0 \qquad x(0) = 0 \tag{52a}$$

$$\dot{y} = \alpha \cos(\omega_c t+\theta) - \frac{E}{B} \qquad y(0) = 0 \qquad \alpha \cos\theta - E/B = v_s \cos\varphi \tag{52b}$$

$$\dot{z} = \alpha \sin(\omega_c t+\theta) \qquad z(0) = 0 \qquad \alpha \sin\theta = v_s \sin\varphi \tag{52c}$$

These three equations have the following solutions, according to the values of the electric field and the starting velocity:

$$\begin{pmatrix} x(t) \\ y(t) \\ z(t) \end{pmatrix} = \frac{\alpha}{\omega_c} \begin{pmatrix} 0 \\ \sin(\omega_c t+\theta) - \sin\theta - \frac{eE}{\alpha m} t \\ \cos\theta - \cos(\omega_c t+\theta) \end{pmatrix} \tag{53}$$

We will now determine the magnetic field which does not allow the electron to cross the region. We therefore demand that when z equals L, the velocity in the z-direction is zero, and that when z = L/2 the velocity in the z-direction is v^*. This specific velocity will proove to be closely related to the resonance in the well.

$$v_z = 0 \quad \longrightarrow \quad \omega_c t + \theta = \pi \tag{54}$$

Using Eq.(54) in z = L yields:

$$\omega_c = \frac{\alpha}{L} (1 + \cos\theta) \tag{55}$$

In the same way use $v_z = v^*$ when z = L/2:

$$\alpha^2 = \alpha^2\cos^2\theta - \alpha\omega_c L\cos\theta + \frac{1}{4}\omega_c^2 L^2 + (v^*)^2 \tag{56}$$

Solving Eq.(55) with Eq.(56) yields for the magnetic field:

$$B_{stop} = \frac{mv^*}{eL}\sqrt{\frac{4(1+\cos\theta)}{3-\cos\theta}} \tag{57}$$

Of course both v^* and the angle θ depend on the electric field. When the electron enters the region with angle $\pi/2$, this special magnetic field is the solution of:

$$\frac{mE}{eB^2}\left(1 + \frac{1}{\sin\left[\arctan\left(\frac{E}{v_s B}\right)\right]}\right) = L \tag{58}$$

We solve Eq.(58) with Newton's method. The results are shown in Fig.9. We took for L the length of our structure (the two barriers and the well) which is about 164 Å. The magnetic field at which no current is possible is calculated for three values of v_s, namely $v_s = 0$ which yields Eq.(55), $v_s = v_0/2$, $v_s = v_0$, where v_0 is the velocity according to the energy E_0, which is the velocity in the z-direction in the well. The electric field is given in units volt per L, where L is the length of the structure.

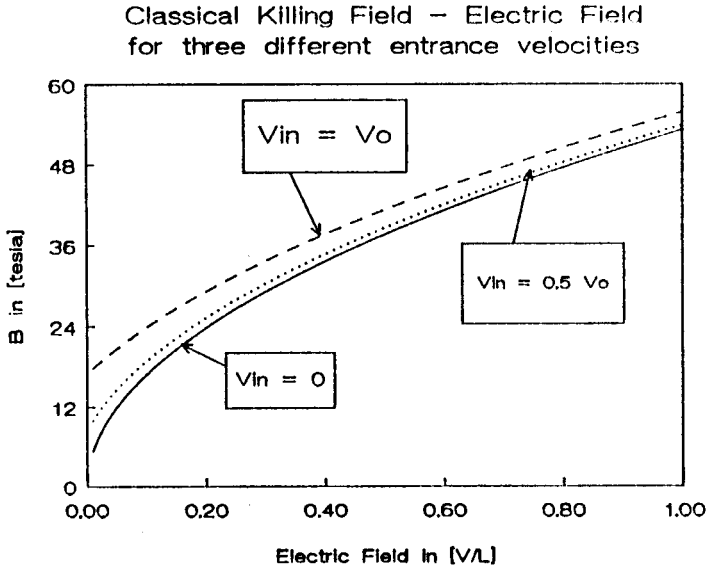

Figure 9 The classical killing field as a function of the electric field in the region. The parameters are accounted for in the text.

There seems to be no such thing as a killing field in classical electrodynamics: no matter how large the magnetic field, there is always an electric field possible which allows current.
When we consider our Double Barrier structure, the only allowed velocity in the z-direction in the well is according the resonance energy E_0:

$$v^* = \sqrt{2E_0/m} \tag{59}$$

Eq.(57) is maximal for $\theta = 0$. For this value of B, no electron will propagate further than z=L. This value of B is:

$$B = \frac{1}{eL}\sqrt{8mE_0} \tag{60}$$

which is shows excellent agreement with the quantum mechanical expression of Eq.(46a).

4. RESULTS

4.1 Current density and charge density in the well versus voltage as a function of the magnetic field.

As is clear from the previous chapters, it is necessary to use an iterative scheme to perform selfconsistent calculations, because Schrödinger's equation and Poisson's equation are coupled. Therefore to get J_z-V_b and n_{3w}-V_b characteristics at various values of the transverse magnetic field, the help of a computer is indispensable.

The program has a similar set up as the one used in the zero-field case. The only difference is that now we have to treat each k_y separately and in order to calculate the current we have to determine what part of the electrons in the well participate in the current. The computer program works according to Fig.10, which is a sort of flow chart of the program.

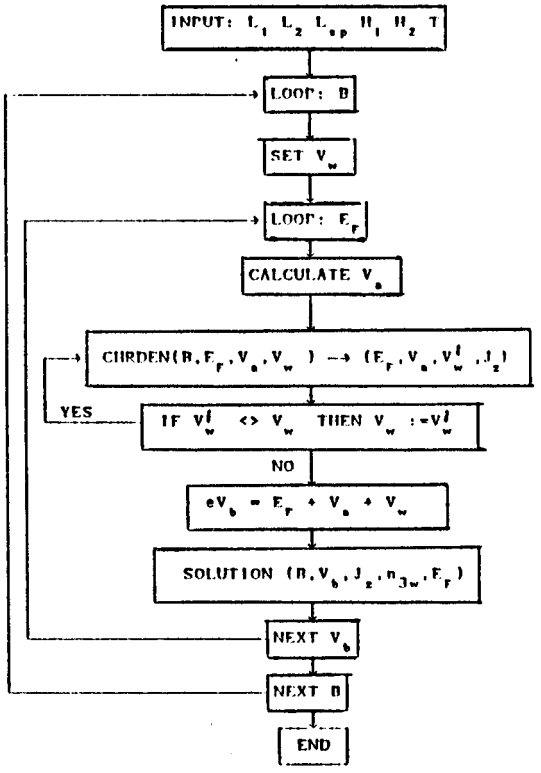

Figure 10 A "flow chart" of the program that calculates in a selfconsistent way the current density and the electron density in the well as a function of the bias voltage at fixed values of the magnetic field.

We start the loop of the magnetic field. For each value of the magnetic field we start another loop: that of the Fermi energy. For each Fermi energy we seek the selfconsistent solution of Schrödinger's and Poisson's equation by means of interval bisection: At fixed E_F we calculate the electron density in the left spacer, and with that we calculate V_a, the potential drop across the first barrier. We choose a value for V_w, which is usually V_a or the value for V_w calculated with the previous E_F, and calculate with the values of (B, T, E_F, V_a, V_w) by means of a procedure CHRDEN the electron density in the well n_{3w} and the current density J_z. With n_{3w} we calculate a new value for V_w. If this new value differs less than 0.01 % from the old value, the process is stopped. If it differs more, a new value for V_w is chosen by means of interval bisection and start the process starts again. The selfconsistent solution contains this set of numbers: (E_F, V_a, V_w, n_{3a}, n_{3w}, J_z).

We calculated for our symmetric structure selfconsistent J_z-V_b characteristics for different values of the magnetic field. Figure 11 shows the current voltage characteristics at T = 77 Kelvin for the following values of B: 0, 5, 10, 20, 24, 25 and 26 T.

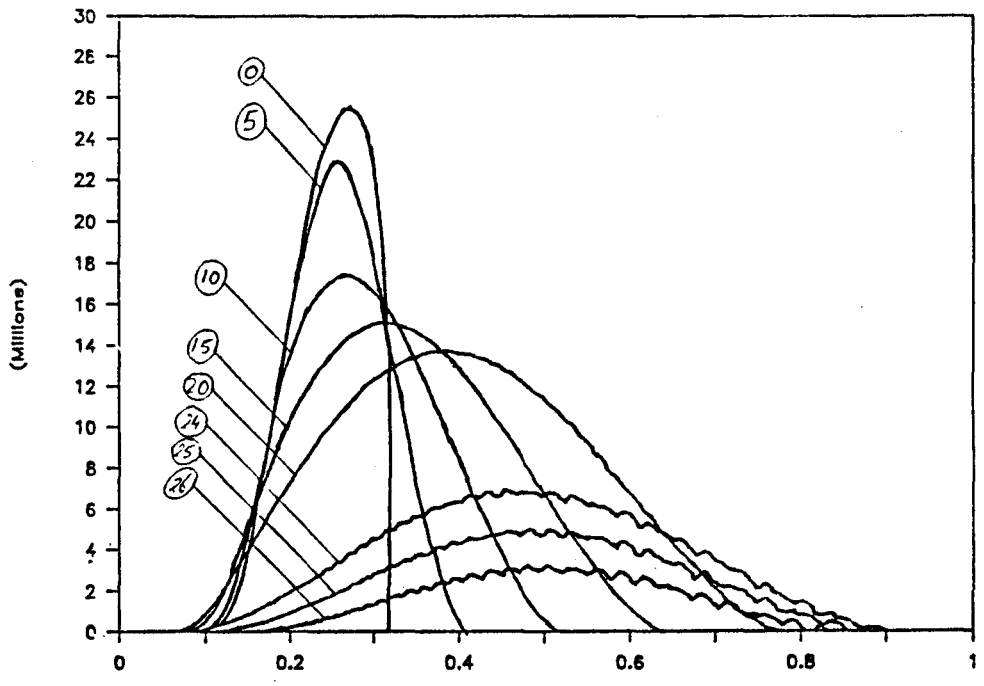

Fig. 11. Current voltage characteristics of a symmetric DBRT structure at T = 77 K. Horizontal V_b in [V], vertical J_z in [A/m^2].

The ripple on the curves is due to the discretisation that is inevitable in numerical integration. Thus it is a manifestation of a numerical and not a physical phenomenon.

The start- and end- voltages, determined from Fig.11, are plotted in Fig.12, together with the predicted values of the previous chapter. It shows that our assumption of no charge in the well is only valid for magnetic fields smaller than 15 T. For higher values of B, the start- and end- voltages deviate from the predicted ones. For B is greater than or equal to 30 T no current is possible, so apparently the killing field is smaller than we predicted in section 3.3.

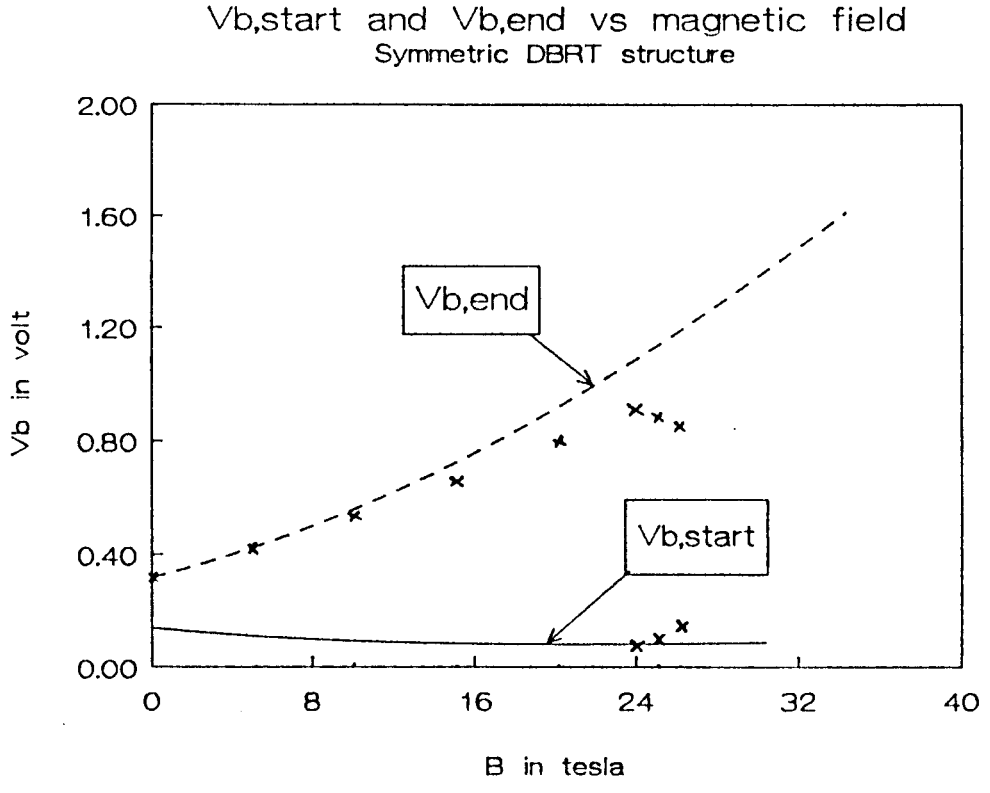

Fig.*12 The start- and end- voltages, for a symmetric DBRT structure at T = 77 K. The values determined from the selfconsistent calculations are indicated by* x, *the predicted values are the solid lines.*

Figure 13 shows the magnetic field dependence of the n_{3w} versus V_b characteristics. When we compare the J_z-V_b with the n_{3w}-V_b curves, it is obvious that the charge in the well accumulates dramatically for magnetic field greater than 20 T. For a magnetic field greater than 15 T, the maximum current decreases with B, whereas the electron density in the well increases. This explains why our predicted values of the start and end voltages deviate from the calculated values.

For magnetic fields greater than 15 T it is not realistic to neglect the charge in the well. At about 24 T the start voltage is greater than the predicted value, and the end voltage is considerably smaller than the predicted value. It is difficult to explain why this happens, because it is impossible to tell what the selfconsistent effect of charge in the well is on these values. Assuming that this is not an effect of selfconsistency, we could explain it by the fact that at 24 T another inequality becomes dominant. We will return to this subject in the next chapter.

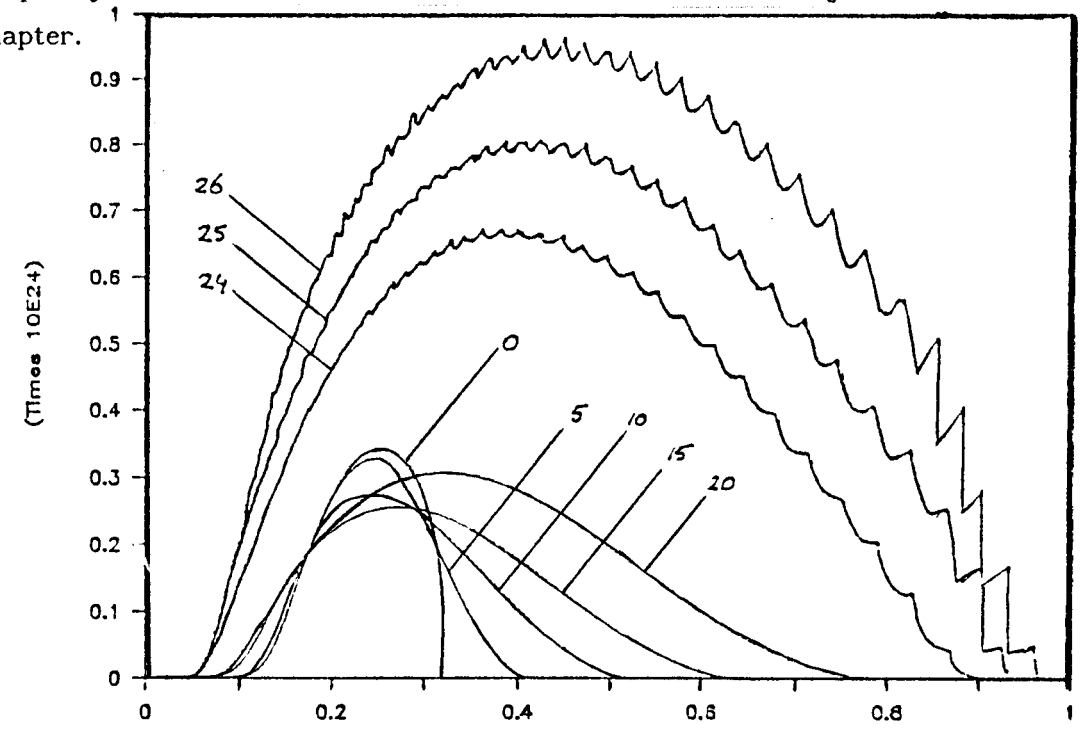

Figure *13 The electron density in the well, in* m^{-3}, *versus bias voltage,* in *V, for different values of the magnetic field, calculated in a selfconsistent way, at T = 77 Kelvin. Note that the maximum electron density in the well increases with the magnetic field, when B becomes larger than 15 T.*

4.2 Current density and electron density in the well as a function of the magnetic field at fixed bias voltage.

As Fig.11 shows, current can flow when B ≠ 0 at voltages that did not have current in the B = 0 case. To examine more closely this behavior as well as to examine the existence of a killing field, we calculate current density and electron density in the well as a function of the magnetic field at three fixed bias voltages (T=4.2 K): at 0.1 V, which is about the start-voltage in the zero field case; at 0.2 V, which is close to the peak current in the zero-field case; and at 0.33 V, which is just below the zero-field $V_{b,end}$. The behavior of the DBRT at these three voltages is very elucidating with respect to the effect of the magnetic field.

The algorithm is similar to the one described in the previous section. Instead of the demand of a constant Fermi-energy we now demand a constant bias voltage which means that we must vary E_F instead of V_b. Thus we keep the bias voltage fixed and we can vary at each voltage the magnetic field. The "flow-chart" of the program is similar to Fig.10; only the two loops must be switched.

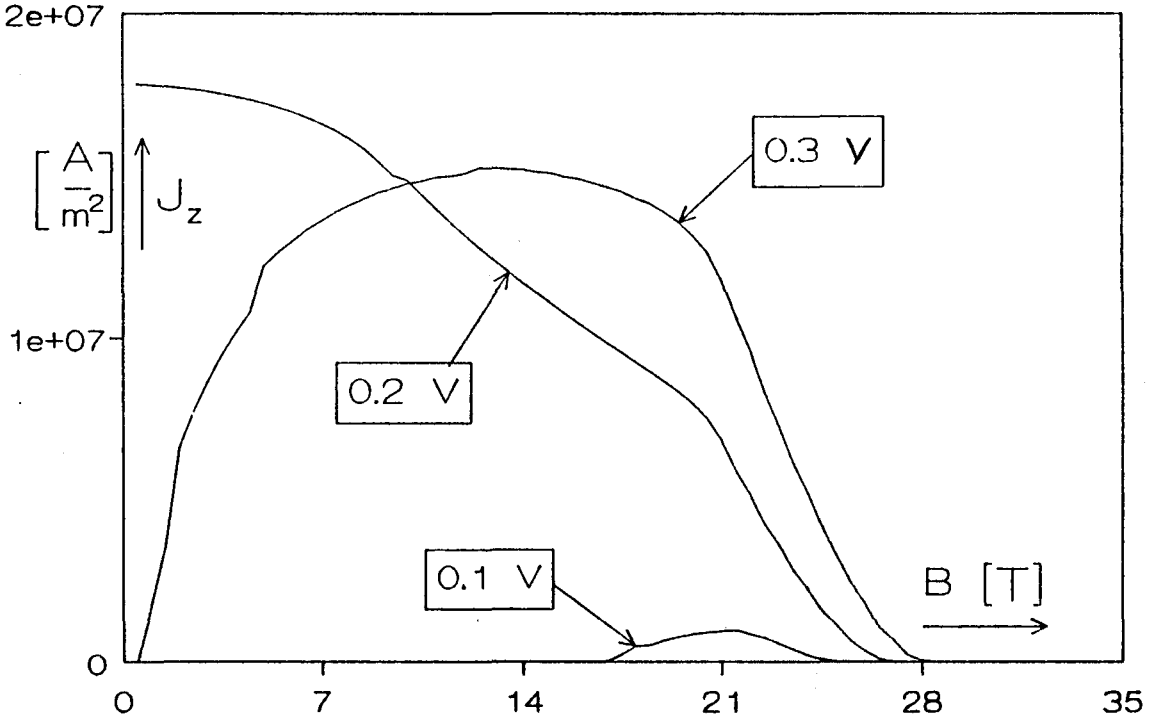

Figure *14: Selfconsistent calculation of the current density as a function of the magnetic field for three fixed applied bias voltages, at T = 4.2 K.*

At a fixed bias voltage of 0.1 V, there is no current at zero magnetic field, whereas at higher magnetic fields, a current does exist. The current at a fixed bias voltage of 0.2 V decreases monotonously with the magnetic field. It appears that the killing field is not completely independent of V_b. However, the variation with V_b is very small. No current is found at any value of V_b for B greater than 28 T, a value of the killing field that is somewhat smaller than the predicted 34 T. The reason why it is smaller can be found in the electron density in the well (see Fig.15).

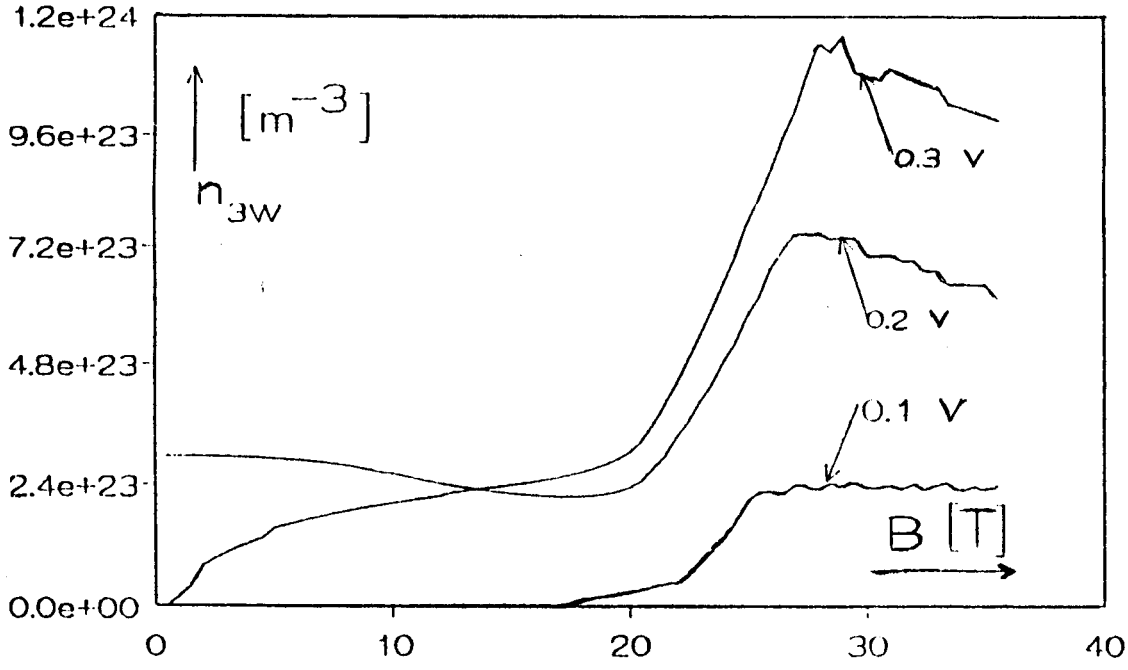

Figure 15: Selfconsistent calculation of the electron density in the well versus the magnetic field, at three fixed applied bias voltages, when T = 4.2 Kelvin. Note that the electron density in the well decreases monotonically with B when B is greater than some 28 T.

Figure 15 shows that for magnetic fields greater than 20 T, the electron density in the well increases dramatically with the magnetic field up to B_{kill}. For yet larger magnetic fields the electron density in the well decreases again. The ripples are again due to the discretisation in the numerical integration over k_y.

Although our predictions are based on neglecting the charge in the well, they give much insight in the magnetic field dependent behavior of the DBRT. We expected the charge in the well to become very important when the magnetic field is such that very few electrons can participate in the current (in that case for very few electrons the resonance level lies above the conduction band minimum of the right spacer) whereas a lot of electrons enter the well. This is the main difference with the zero-field case, because there the charge build up in the well is always balanced by a constant out stream in the collector.

In the next chapter we will evaluate the results and the model, specifically the approximations we made regarding the magnetic field.

5. DISCUSSION AND CONCLUSIONS

5.1 Discussion

In this chapter we discuss the results of the previous chapter and use them to discuss the model approximations we made, specifically those regarding the magnetic field. Also we compare our results with others, and draw some conclusions.
First we will discuss the model approximations made in the zero field case and the additional approximations we made in the non-zero field case:

Approximations made in the zero-field case.

1. Only coherent propagation of electrons is considered. This means that electrons are described by the solutions of a Schrödinger-like envelope equation, in which we use one effective mass, namely that of GaAs in the Γ-band minimum. We do not deal with the effective mass problem, because our main goal is to develop a simple model which explains the most important physics of the DBRT.
2. We only consider resonant current, so we neglect the electrons that tunnel non-resonantly into the well. Consequently, our I-V curves show no nonresonant background current and our model is unable to yield a peak-to-valley ratio. The profit from the restriction to resonant contributions only is that an integration over k_z (in current and charge densities) is avoided. This simplifies calculations a lot, because the resonance is now described by a delta function of the transmission coefficient (as a function of the electron energy).
3. Only tunneling from left to right is considered and the Fermi sea in the right spacer is neglected. In structures for which $E_0 \gg E_F$ this assumption is quite reasonable, because electrons from the collector can not traverse resonantly when V_b is such that emitter electrons can.
4. We neglect "sequentializing" phenomena such as phonon interaction and elastic or inelastic scattering from defects etc. At sufficiently low temperature and in structures with clean intrinsic layers, these

influences are minimized.

5. The Fermi level depends heavily on the applied voltage. This reflects the semiconductor character of the spacer layer, but it does not give the metal character of the doped reservoir it is due to. This aspect of the model yields too small E_F values at high bias.

6. The potential drop in both emitter and collector layers is neglected. Here, a dependence of the potential on the doping density can be expected. As a consequence, our voltage scale in the I-V curves can not be taken seriously. However, we expect our V_b to be related to the "true" voltage by a smooth and monotonous transformation.

7. We model the potential energy caused by the band bending by a piece-wise constant one: in the two barriers and the well we take its mean value. This has the advantage that the electron wave functions are simple plane waves. Differences with Airy function calculations [14] are so small, that this simplification is well justified.

Additional approximations with respect to the magnetic field

1. The magnetic field is confined to the two barriers and the well only. This is mainly done to avoid complication of the calculation of the electron density in the left spacer with a larger field region: the wave functions would be parabolic cylinder functions, of which no integrals are known analytically. As a consequence the field scale in the I-B curves can not be taken seriously. A further consequence is related to the fact that in our model the B-region exactly coincides with that of the electric field. If we drop this special choice, the expression for the killing field is complicated. Also, its non-dependence of V_b disappears. In fact, configurations can be devised that have no finite killing field.
With this approximation we introduce discontinuities in the vector potential and its curve. It would be more realistic to choose both quantities continuous differentiable by "rounding off their profiles".

2. The second approximation we made with respect to the magnetic field is analogous to approximation 7 of the zero field model: we make the potential energy caused by the magnetic field piece wise constant, although the potential energy is a quadratic function of the magnetic

field B. Again we take the mean value of the potential energy in the two barrier and the well.

Confrontation of zero-field and nonzero-field approximations

The second approximation regarding the magnetic field results in working with plane wave instead of parabolic cylinder functions, which is a great difference in mathematics, whereas the calculated transmissions differ about 2%. Therefore this approximation is not the most serious one.
The first approximation regarding the magnetic field, is more interesting. The confinement of the magnetic field to the two barriers and the well does not have any physical grounds. We merely confined the magnetic field to this limited region because thus the magnetic field does not not affect the calculation of the electron density in the left spacer. It would be more realistic to confine the magnetic field to a larger region.
One of the consequences of a larger region of confinement is that the killing field will be smaller than the 28 T we calculated. If Eq.(58) still applies, B_{kill} is inversely proportional to the length of the field region L. Also, our predicted values for the start- and end- voltages would change, but the shape of the curves of Fig.7 will be the same.
The analysis of the start- and end- voltages as described in section 3.2 is hindered by the fact that our Fermi energy changes with V_b. Therefore it is impossible to tell whether the sudden change in behavior of the two voltages at $B \approx 24$ T is due to selfconsistency. The freely tunable Fermi level is a way to take the effects of an applied bias voltages into account in the zero field model. However, when the Fermi level is taken a constant, so the range of k_y is no longer variable, the equations are much simpler to solve.
It appears that then the predicted values of the start- and end- voltages are very close to the ones depicted with "x" in Fig.12 , which would mean that the deviation of the voltages from the solid lines in Fig.12 is not totally a selfconsistent effect [28].

Finally, we will compare our results with the work of others.

As the work on resonant tunneling with a transverse magnetic field is concerned, we will compare our results with that of Ancilotto [26], Brey, Platero and Tejedor [23], and Eaves *et al.* [7].

First we will mention the work on transverse magnetic fields in general to see whether the ideas mentioned can help us further. We mention the work on transverse magnetic fields and semiconductor structures in general by: Guéret, Baratoff and Marclay [29], Hickmott [30], Johnson, MacKinnon and Goebel [20], Sheard *et al.* [4], and Maan *et al.* [21], [31], [32], and Altarelli and Platero [24], [33].

References [22], [24], [26] and [33] mention the parabolic cylinder functions (or confluent hypergeometric functions) as solutions of the Schrödinger equation for an electron in a transverse magnetic field. They use large computer facilities, [33], to calculate transmission characteristics of single barriers, to analyze magnetic hole levels, or to describe Landau levels near an ideal interface. They indicate to have had some problems in calculating these special functions.

References [21], [31], and [32], try to explain the physics of tunneling in terms of skipping orbits and other classical terms. Of course these kind of considerations can give a lot of insight, but as tunneling is regarded, one can not leave out quantum mechanics.

References [24] and [29] use a generalized transfer Hamiltonian method to describe the magneto tunneling. They solve the Schrödinger equation purely numerical, which is not wrong, but dealing with piece wise constant potentials (plane wave) will elucidate the physics of tunneling more.

None of the references deals with the problem of confining the magnetic field, all confine the magnetic field to just one barrier (in the case of single barrier tunneling [29]) or the two barriers. All refer to Büttiker [25], who confined the magnetic field to the barriers.

We now try to compare our results to the available theoretical or experimental data on DBRT structures.

Reference [26] uses parabolic cylinder functions to calculate the I-V characteristics of a structure with barriers 200 Å wide and 0.04 eV high and a well 30 Å wide. The calculations are not selfconsistent and the results are that the start and end voltages do not change with the magnetic field. The maximum current decreases with the magnetic field. When we apply our model on this structure we also find hardly changing start- and end- voltages. Therefore we conclude that the model used in reference [26] is not wrong with respect to the treatment of the magnetic field, but the structure used is not very revealing.

References [24] and [33] concentrate on oscillations in the current as a function of the magnetic field, without calculating selfconsistently. The fact that they look at oscillations hints at the existence of more than one level in the well, which undermines coherence.

Reference [23] present magneto tunneling calculations on superlattice-barrier-superlattice structures, that can, to some extent, be compared with our DBRT. The behavior of the first resonance peak in their I-V curves shows good agreement with our calculations of the resonant current.

Finally we discuss [34] which shows current-voltage characteristics of a structure comparable to the one we use (AlGaAs barriers and GaAs well are 55 Å wide). Their maximum current shifts to higher bias voltages with increasing magnetic fields, but the curve drowns in the non resonant current contribution.

Unfortunately, no experimental data of configurations as considered, are presently available. Eaves et al. [7], have investigated structures with wide wells having many resonance levels. Both facts are related to the difficulties involved in confining a transverse magnetic field enough to still have output.

5.2 Conclusions

The transverse magnetic field

A transverse magnetic field causes the tunnel problem to become dependent on k_y, in the gauge we took. Related to this choice of gauge is the fact that the wave number k_y changes discontinuously when the wave function of the electron crosses a discontinuity in the vector potential. This means that the boundary conditions we encounter in calculating the electron wave function throughout the structure are different from the zero field case. This also means that the calculation of electron densities is complicated; the integral over k_y can not be performed analytically, as in the zero field case, but must be performed numerically.

The solutions of the Schrödinger equation for an electron in a transverse magnetic field are in general parabolic cylinder functions (also known as confluent hypergeometric functions), which only give rise to a quantization of energy (Landau levels) when no boundaries are present, because boundaries can make all unbounded parabolic cylinder functions square integrable. The fact that a lot of these function are unbounded makes them difficult to work with. In this report we could avoid them by modeling the potential energy term, introduced by the magnetic field, as a piece-wise constant one.

Results of the model

The model, based on wave coherence and selfconsistent calculation of charge, explains the intrinsic bistability of a DBRT structure in the zero field case, as well as the magneto oscillations in the $\underline{B} \parallel \underline{J}$ case.

In the $\underline{B} \perp \underline{J}$ case this model predicts interesting features of the magnetic field dependence of both charge and current:

The maximum current decreases monotonously with the magnetic field, but occurs at higher bias voltages. When the killing field ($B \approx 28$ T for our structure) is reached, no resonant current is possible up to 1.0 V. Due to charge build up in the well, a different voltage has a different killing field; At a certain (not investigated) voltage the killing field will

reach a maximum. This maximum will be greater than the predicted 34.2 T.

The voltages at which the resonant current starts or ends change with the magnetic field. The start voltages decreases monotonously with the magnetic field until B ≈ 24 T. For larger values of the magnetic field, the start voltage increases with the magnetic field. The end voltage increases monotonously with B, but for magnetic fields larger than 24 T, it decreases in the selfconsistent calculation.

Contrary to the current density, the charge density in the well increases with B, and grows rapidly from 20 T up to the killing field. When the magnetic field is larger than the killing field, the charge will slowly disappear from the well.

The merits of the model

The assumptions made in the zero field case still hold when a transverse magnetic field is present.

The confinement of the magnetic field is a problem yet to be investigated. However, we think that a large field region does not introduce new elements in the physics. In that case there is also a killing field, but it will be smaller than the 34.2 T we predict. The magnetic field dependence of the start- and end- voltages will be the same, only the values of the magnetic field will be different.

Our modeling of the potential energy as a piece-wise constant one enables an analysis of the current condition which led to a prediction of the start- and end- voltages as well as the killing field, which is solely dependent of the parameters of the structure (with E_0 the resonance energy measured from the bottom of the well, m the effective mass of an electron in the Γ minimum of GaAs, L_1 the width of the first barrier, L_2 the width of the second barrier, and L_w the width of the well):

$$B = \frac{1}{e}\left(\frac{4mE_0}{L_w(L_1+L_2+L_w/3)+2L_1L_2}\right)^{1/2}$$

REFERENCES

[1] L. Esaki, and R. Tsu, IBM Res. Note, RC-2418, Mar. 1969

[2] L. Esaki, and R. Tsu, IBM J, Res. Develop., pp 61-65, Jan.1970

[3] H.J.M.F. Noteborn, H.P. Joosten, and D. Lenstra, Phys. Script. T.33 p.219 (1990)

[4] F.W. Sheard, K.S. Chan, G.A. Toombs, L. Eaves, and J.C. Portal, Int. Phys. Conf. Ser. No.91: Chapter 4, paper presented at Int. Symp. GaAs and related compounds, Heraklion, Greece, 1987

[5] F.W. Sheard, and G.A. Toombs, Appl.Phys.Lett.52, 1228, 1988

[6] P.J. van Hall, and J.H. Wolter,"The use of imaginary potential in DBRT-diodes", paper presented at the 5th Int. Conf. on the physics of electro-optic microstructures and microdevices, Heraklion, Crete, Greece, July 30 - August 2, 1990

[7] L. Eaves, E.S. Alves, M. Henini, O.H. Hughes, M.L. Leadbeater, C.A. Payling, F.W. Sheard, G.A. Toombs, A. Celeste, J.C. Portal, G. Hill, and M.A. Pate, "The Application of High Magnetic Fields in Semiconductor Physics", Würzburg, Aug.22-26, 1988

[8] H.J.M.F. Noteborn, G.H.M. van Tartwijk, H.P. Joosten, and D. Lenstra, to be published in Journal of Physics C.

[9] M.G. Burt, Semicond. Sci. Technol., 3, 739 (1988)

[10] B. Zimmermann, E. Marclay, M. Ilegems, and P. Guéret, J.Appl.Phys. 64, 7 (1988)

[11] R. Landauer, in "Localization, Interaction and Transport Phenomena", eds. B. Kramer, G. Bergmann, and Y. Bruynserade, p.38, Springer, Heidelberg, 1985

[12] M. Büttiker, Y. Imry, R. Landauer, and S. Pinhas, Phys.Rev.B., 31, 6207 (1985)

[13] M.Ya. Azbel, Phys.Rev.B. 28, 4106 (1983)

[14] H.P. Joosten, H.J.M.F. Noteborn, and D. Lenstra, Internal Report, Eindhoven University of Technology (1989)

[15] J.S. Blakemore, "Semiconductor Statistics", Pergamon Press, Oxford - London - New York - Paris, 1962

[16] S. Gasiorowicz, "Quantum Physics", Chapter 13, Wiley, New York, 1974

[17] M. Abramowitz, and I.A. Stegun, Handbook of Mathematical Functions, Chapter 19, Dover Publ., New York 1965

[18] J. Spanier, and K.B. Oldham, An Atlas of Functions, Chapter 46, Springer, Berlin, 1987

[19] A. Erdelyi, W. Magnus, F. Oberhettinger and F.G. Tricomi, "Higher Transcendental Functions, Vol.II, Chapter 8, McGraw-Hill Book Company, New York - Toronto - London, 1953

[20] E.A. Johnson, A. MacKinnon, and C.J. Goebel, J.Phys.C. **20** (1987), L521-L525

[21] J.C. Maan, in "Magnetic Quantization in Superlattices", Festkörperprobleme/Advances in Solid State physics 27, Ed. P. Grosse, Friedr. Vieweg & Sohn, Braunschweig/Wiesbaden 1987

[22] J. Spanier, and K.B. Oldham, An Atlas of Functions, Chapter 24, Springer, Berlin, 1987

[23] L. Brey, G. Platero, and C. Tejedor, Phys.Rev.B, 38, 14, 9649, (1988)

[24] M. Altarelli, and G. Platero, Superl. and Micro-struct., Vol.5, No.4, 1989

[25] M. Büttiker, Phys.Rev.B, 27, 10, 6178 (1983)

[26] F. Ancilotto, J.Phys.C.: Solid State Phys. **21**, 4657 (1988)

[27] F. Ancilotto, A. Selloni, and E. Tosatti: Phys.Rev.B 40, 6, 3729 1989

[28] H.J.M.F. Noteborn, private communication, nov.1990

[29] P. Guéret, A. Baratoff and E. Marclay, Europhys.Lett. 3 (3) 367, 1987

[30] T. W. Hickmott, Solid State Comm., Vol.63, No.5, 1987

[31] J.C. Maan, Surf.Sci. 196, 518 (1988)

[32] G. Belle, J.C. Maan, and G. Weimann, Surf.Sci. 170, 611 (1986)

[33] M. Altarelli, and G. Platero, Surf.Sci. 196, 540 (1988)

[34] S. Ben Amor, K.P. Martin, J.J.L. Rascal, R.J. Higgins, A. Torabi, H.M. Harris, and C.J. Summers, Appl.Phys.Lett. **53**, 25, 1988

[35] S. Gasiorowicz, "Quantum Physics", Chapter 5, Wiley, New York, 1974

[36] W. Greiner,"Quantum Mechanics, An Introduction", Chapter7, pg.111, Springer-Verlag Berlin Heidelberg 1989.

[37] L.D. Landau, and E.M. Lifshitz, Quantum Mechanics, Course of Theoretical Physics, Volume 3, "Quantum Mechanics", p.425, Pergamon Press, Oxford, London, Edinburgh, New York, Paris, Frankfurt, 1965

APPENDIX A: THE PARABOLIC CYLINDER FUNCTIONS

A.1. Introduction

In this Appendix, we will discuss the solutions of the Schrödinger equation with gauge $\underline{A}$ = (0,-Bz,0), known as parabolic cylinder functions. One of the problems one encounters in dealing with special functions is that they all seem to be expressed in each other. Further, in previous work on transverse magnetic field, it was merely stated that it is difficult to calculate accurate values of this special function. Exemplary for this is a paper by M. Altarelli and G. Platero [33], where it is stated that "the basic problem for the numerical calculations is the accurate determination of the confluent hypergeometric functions, which can be achieved by a combination of integral representations, recursion relations and asymptotic expansions".

In this Appendix we will give a selection of those representations, relations and expansions as encountered in various textbooks on special functions, because the textbooks are usually so loaded with integral expressions, asymptotic expansions and recursion formulas that its difficult to see what type of relation one specifically needs. To create some order out of this chaos and to find the relations that enable us to compose an easy and fast algorithm for calculating the parabolic cylinder functions are the main goals we set ourselves in this Appendix.

We start with a very basic problem, which proves to be an excellent entry in the field of the parabolic cylinder functions. After that we will mention some representations, recursion relations and asymptotic expansions, discussed in *Handbook of Mathematical Functions*, by Abramowitz and Stegun, [17], which we will call [A&S], *The Atlas of Functions*, by Spanier and Oldham, [18], to which we will refer as [S&O], *Higher Transcendental Functions*, by Erdélyi, Magnus, Oberhettinger, and Tricomi, [19], which we will call [EMOT]. Also we will use *Quantum Mechanics*, by E. Merzbacher, [MB].

A.2. The harmonic oscillator

We start with a basic but very illustrative problem; that of the harmonic oscillator. Its potential energy is $V(x) = \frac{1}{2}m\omega^2x^2$. We call ω loosely the (classical) frequency of the oscillator. Such a parabolic potential is of great practical importance because it approximates any arbitrary potential in the neighborhood of a stable equilibrium position. Another reason why the linear harmonic oscillator is of great practical importance is the fact the behavior of most continuous physical systems, such as the vibrations of an elastic medium, or the electromagnetic field in a cavity, can be described by the superposition of an infinite number of simple harmonic oscillators. In the quantization of any such physical system we are then confronted by the quantum mechanics of many linear harmonic oscillators of various frequencies.

The Schrödinger equation:

$$\frac{-\hbar^2}{2m}\frac{d^2}{dx^2}\Psi + \frac{1}{2}m\omega^2x^2\Psi = E\,\Psi \qquad (A.1)$$

can be transformed into a convenient form by substituting $\xi = (m\omega/\hbar)^{1/2}x$:

$$\frac{d^2}{d\xi^2}\Psi + \left(\frac{2E}{\hbar\omega} - \xi^2\right)\Psi = 0 \qquad (A.2)$$

If a power series solution of this equation is attempted a three-term recursion formula is obtained. To get a differential equation where the power series solution admits a two-term recursion relation, which is simpler to analyze, we substitute $\Psi = \exp(-\xi^2/2)g(\xi)$, which yields for g:

$$\frac{d^2}{d\xi^2}g - 2\xi\frac{dg}{d\xi} + 2\left(\frac{E}{\hbar\omega} - \frac{1}{2}\right)g = 0 \qquad (A.3)$$

In the harmonic oscillator problem the solutions $g(\xi)$ have only a physical meaning if they are square integrable, which means that they have to be bound on the interval $\xi \in (-\infty,\infty)$. A direct result of this demand is a quantization of energies; only the power series which have $E = (n+\frac{1}{2})\hbar\omega$, with n a nonnegative integer, satisfy this condition. The eigen functions of the linear harmonic oscillator problem are called *Hermite polynomials* of

degree n.

The complete eigen functions are of the form:

$$\psi_n = C_n H_n(\xi)\exp(-\xi^2/2) \qquad C_n = 2^{-n/2}(n!)^{-1/2}\left(\frac{m\omega}{\hbar\pi}\right)^{1/4} \tag{A.4}$$

where H_n denotes a Hermite polynomial of degree n, and C_n is a normalization constant. The Hermite polynomials are expressed in power series ϑ_1 and ϑ_2:

$$H_n(\xi) = (-1)^{n/2}\frac{n!}{(n/2)!}\vartheta_1(\xi) \qquad \text{n is even} \tag{A.5a}$$

$$H_n(\xi) = (-1)^{(n-1)/2}\frac{2(n!)}{[(n-1)/2]!}\vartheta_2(\xi) \qquad \text{n is odd} \tag{A.5b}$$

where ϑ_1 and ϑ_2 are the power series:

$$\vartheta_1 = 1 - \frac{2n}{2!}\xi^2 + \frac{2^2n(n-2)}{4!}\xi^4 - \frac{2^3n(n-2)(n-4)}{6!}\xi^6 + \ldots \tag{A.6a}$$

$$\vartheta_2 = \xi - \frac{2(n-1)}{3!}\xi^3 + \frac{2^2(n-1)(n-3)}{5!}\xi^5 - \ldots \tag{A.6b}$$

Note that the power series (A.6a) and (A.6b) are special cases of the complete set of mathematical solutions of the harmonic oscillator problem. For instance, if we no longer demand that the potential is present on an infinite interval, but on a finite one, all power series can be ascribed a physical meaning, because they all are square integrable on a finite interval.

The complete set of solutions of Eq.(A.3), regardless their behavior on the interval $(-\infty,\infty)$ is usually called the set of parabolic cylinder functions, but are also known as Weber functions or Weber-Hermite functions. In the next section we will elaborate on these more general solutions of the harmonic oscillator problem.

A.3. The parabolic cylinder equation

We are looking for the complete set of solutions of the differential equation:

$$\frac{-\hbar^2}{2m}\frac{d^2}{dx^2}\Psi(x) + \frac{1}{2}m\omega^2x^2\Psi(x) = E\,\Psi(x) \qquad (A.7)$$

With the substitution $z = (2m\omega/\hbar)^{1/2}x$ and $E = (\nu+\frac{1}{2})\hbar\omega$ Eq.(A.7) transforms to:

$$\frac{d^2}{dz^2}\Psi + \left(\nu + \frac{1}{2} - \frac{z^2}{4}\right)\Psi = 0 \qquad (A.8)$$

This differential equation is known as Weber's equation [SO]. Its solutions are the parabolic cylinder functions:

$$D_\nu(z),\quad D_\nu(-z),\quad D_{-\nu-1}(iz),\quad D_{-\nu-1}(-iz) \qquad (A.8a)$$

If ν is not an integer the first two are linearly independent. For all values of ν, $D_\nu(z)$ and $D_{-\nu-1}(\pm iz)$ are linearly independent. Because in our problem ν can be a nonnegative integer (the former quantization energies), we use $\langle D_\nu(z), D_{-\nu-1}(iz)\rangle$ as linear independent set of solutions. To get an idea, of the behavior of these functions table A.1 gives some facts about $D_\nu(z)$.

	$D_\nu(-\infty)$	$D_\nu(0)$	$D_\nu(\infty)$
$1<\nu<2,\ 3<\nu<4,\ 5<\nu<6,\ldots$	$+\infty$	$\dfrac{(2^\nu\pi)^{1/2}}{\Gamma\left(\frac{1-\nu}{2}\right)}$	0
$0<\nu<1,\ 2<\nu<3,\ 4<\nu<5,\ldots$	$-\infty$		
$\nu=0,1,2,3,\ldots$	0		
$\nu<0$	$+\infty$		

tableA.1

In table A.1 the functions with $\nu = 0,1,2,3,\ldots$ are the ones that are bound on the interval $-\infty < z < \infty$, the solutions of the harmonic oscillator problem:

$$D_n(z) = 2^{-n/2}\exp\left(\frac{-z^2}{4}\right) H_n\left(2^{1/2}z\right) \qquad (A.9)$$

The functions $D_\nu(z)$ and $D_{-\nu-1}(iz)$ are power series of the kind given by Eq. (A.6a), (A.6b) and are often expressed in a more general class of power series, namely Kummer functions, who are the solutions of the so called *confluent hypergeometric equation.* This Kummer function is often written as M(a;c;z), where the variables a and c are termed the numeratorial and denominatorial parameter, and z is the argument. The advantage of expressing power series in terms of Kummer functions is that the latter are very simple power series:

$$M(a;c;z) = 1 + \frac{az}{c} + \frac{a(a+1)z^2}{2!c(c+1)} + \frac{a(a+1)(a+2)z^3}{3!c(c+1)(c+2)} + .. = \sum_{j=0}^{\infty} \frac{(a)_j z^j}{j!(c)_j} \qquad (A.10)$$

This power series is convergent for all arguments and for all parameter values except c = 0,1,2,.. . The parabolic cylinder function $D_\nu(z)$ is expressed in the Kummer function and in the Γ function by:

$$D_\nu(z) = (2^\nu\pi)^{1/2}\exp(\frac{-z^2}{4}) \left[\frac{M\left(\frac{-\nu}{2};\frac{1}{2};\frac{z^2}{2}\right)}{\Gamma\left(\frac{1-\nu}{2}\right)} - 2^{1/2}z\,\frac{M\left(\frac{1-\nu}{2};\frac{3}{2};\frac{z^2}{2}\right)}{\Gamma\left(\frac{-\nu}{2}\right)} \right]$$

$$= (2^\nu\pi)^{1/2}\exp(\frac{z^2}{4}) \left[\frac{M\left(\frac{1+\nu}{2};\frac{1}{2};\frac{-z^2}{2}\right)}{\Gamma\left(\frac{1-\nu}{2}\right)} - 2^{1/2}z\,\frac{M\left(1+\frac{\nu}{2};\frac{3}{2};\frac{-z^2}{2}\right)}{\Gamma\left(\frac{-\nu}{2}\right)} \right] \qquad (A.11)$$

Expression (A.9) may be convergent for all z, but that does not mean that its numerically stable for all z. To avoid numerical instabilities one can use the recursion relations given in [A&S], [S&O], [EMOT]. Thus one can transform a numerical unfavorable combination of parameters to a better one.

If that does not work, one can try to use asymptotic expansions. However, often these asymptotic expansions are only valid under certain conditions

and in some cases the cure is worse than the disease.Dealing with all these relations one has to keep in mind what specific ranges of arguments are needed. For instance, in the context of this report, the value ν is a function of the total electron energy. The value of z can become very large and very small (depends on k_y and B) but z is always real, so we don't discuss the problems of determining $D_\nu(a+ib)$.
In the next section we will discuss some of the recursion relations discussed in the aforementioned textbooks.

A.4. Recurrence relations

Our basic notation for the parabolic cylinder functions will be the one used in [S&O], [EMOT] and [MB]. In [A&S] another notation is used which can easily be transformed into the first one. Because the parabolic cylinder equation has 2 linearly independent solutions all kinds of linear combinations can be used as a basis of solutions. In [A&S] the functions U(a,z) and V(a,z) are used and are related to the notation $D_\nu(z)$ in the following way (z complex):

$$U(a,z) = D_{-a-\frac{1}{2}}(z) \qquad V(a,z) = \frac{\Gamma(\frac{1}{2}+a)}{\pi}\left\{\sin\pi a\ U(a,z) + U(a,-z)\right\} \qquad \text{(A.12)}$$

The recurrence relations for U(a,z), which are also satisfied by the functions $\Gamma(\frac{1}{2}-a)V(a,z)$, are:

$$U'(a,z) + \tfrac{1}{2}zU(a,z) + (a+\tfrac{1}{2})U(a+1,z) = 0 \qquad \text{(A.13a)}$$

$$U'(a,z) - \tfrac{1}{2}zU(a,z) + U(a-1,z) = 0 \qquad \text{(A.13b)}$$

$$2U'(a,z) + U(a-1,z) + (a+\tfrac{1}{2})U(a+1,z) = 0 \qquad \text{(A.13c)}$$

$$zU(a,z) - U(a-1,z) + (a+\tfrac{1}{2})U(a+1,z) = 0 \qquad \text{(A.13d)}$$

The recurrence relations for V(a,z), which are also satisfied by the functions $U(a,z)/\Gamma(\frac{1}{2}-a)$, are:

$$V'(a,z) - \tfrac{1}{2}zV(a,z) - (a-\tfrac{1}{2})V(a-1,z) = 0 \qquad \text{(A.14a)}$$

$$V'(a,z) + \tfrac{1}{2}zV(a,z) - V(a+1,z) = 0 \qquad \text{(A.14b)}$$

$$2V'(a,z) - V(a+1,z) - (a-\tfrac{1}{2})V(a-1,z) = 0 \qquad \text{(A.14c)}$$

$$zV(a,z) - V(a+1,z) + (a-\tfrac{1}{2})V(a-1,z) = 0 \qquad \text{(A.14d)}$$

Especially Eq.(A.13d) and (A.14d) are useful. When a parabolic cylinder function has a too large order a it can be transformed into a lower order with these two equations. The other six relations are useful when needing the derivative with respect to z, e.g. when calculating the boundary conditions at an interface needed to perform a Transfer Matrix Approach.
In [S&O], no extra information is provided except an argument-addition formula:

$$D_\nu(x+y) = \exp\left(\frac{2xy+y^2}{4}\right) \sum_{j=0}^{\infty} \frac{(-y)^j}{j!} D_{\nu+j}(x) = \exp\left(\frac{-2xy-y^2}{4}\right) \sum_{j=0}^{\infty} \binom{\nu}{j} y^j D_{\nu-j}(x) \qquad \text{(A.15)}$$

Eq.(A.15) does not make things easier in a numerical way because j grows to infinity.
In [EMOT] we find the following relations which express the relationship between the four solutions of Eq.(A.8):

$$D_\nu(z) = \frac{\Gamma(\nu+1)}{(2\pi)^{1/2}} \left[e^{\nu\pi i/2} D_{-\nu-1}(iz) + e^{-\nu\pi i/2} D_{-\nu-1}(-iz) \right] \qquad \text{(A.16a)}$$

$$= e^{-\nu\pi i/2} D_\nu(z) + \frac{(2\pi)^{1/2}}{\Gamma(-\nu)} e^{-(\nu+1)\pi i/2} D_{-\nu-1}(iz) \qquad \text{(A.16b)}$$

$$= e^{\nu\pi i/2} D_\nu(-z) + \frac{(2\pi)}{\Gamma(-\nu)} e^{(\nu+1)\pi i/2} D_{-\nu-1}(-iz) \qquad \text{(A.16c)}$$

and those which can be obtained from these by substituting -z for z. These relations shows how the functions in (A.16a) are connected. The Wronskian determinants, handy for the Transfer Matrix Approach, of the linearly independent solutions $D_\nu(z)$ and $D_\nu(\pm iz)$ are:

$$D_\nu(z)\,\frac{d}{dz}\,D_\nu(-z) - D_\nu(-z)\,\frac{d}{dz}\,D_\nu(z) = \frac{(2\pi)^{1/2}}{\Gamma(-\nu)} \qquad \text{(A.17a)}$$

$$D_\nu(z)\,\frac{d}{dz}\,D_{-\nu-1}(iz) - D_{-\nu-1}(iz)\,\frac{d}{dz}\,D_\nu(z) = -ie^{-\nu\pi i/2} \qquad \text{(A.17b)}$$

Here we conclude our summary of properties of the parabolic cylinder functions. In the next section we continue with the asymptotic expansions which may be useful when an algorithm in spite of the maximal use made of the properties described above, is numerical instable at large values of $|z|$.

A.5. Asymptotic expansions.

Asymptotic expansions are expressions that describe the asymptotic behavior of functions to which they apply. This means that for small values of the arguments of the special functions, the asymptotic expansions may diverge. In this section we describe these expansions as given in a number of textbooks. Besides [A&S], [S&O], [EMOT] and [MB] we also use *The Confluent Hypergeometric Function*, by Buchholz [BH].

What are we looking for? We want to obtain algorithms that, without numerical instabilities, calculate the values of the parabolic cylinder function $D_\nu(z)$ and $D_{-\nu-1}(iz)$ for all ν and for $-\infty < z < \infty$, z real. The expression of the parabolic cylinder function in Kummer functions works just fine in calculating for $D_\nu(z)$ for $\nu < 50$ and $z > -15$ (See Fig.A1 and Fig.A2). More problems are encountered when calculating $D_{-\nu-1}(iz)$ with Kummer functions: for $\nu = 0.9$ instabilities occur at $|z| \approx 8.5$ (See Fig.A3), which is unacceptable, because $\nu = 0.9$ is not an exotic value.

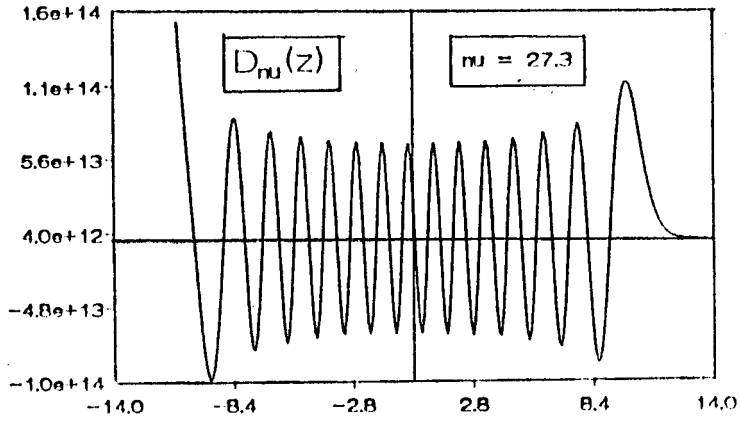

Fig. A1

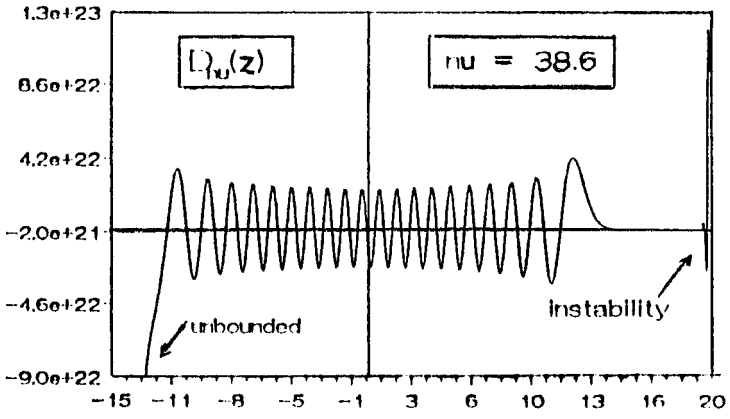

Fig. A2

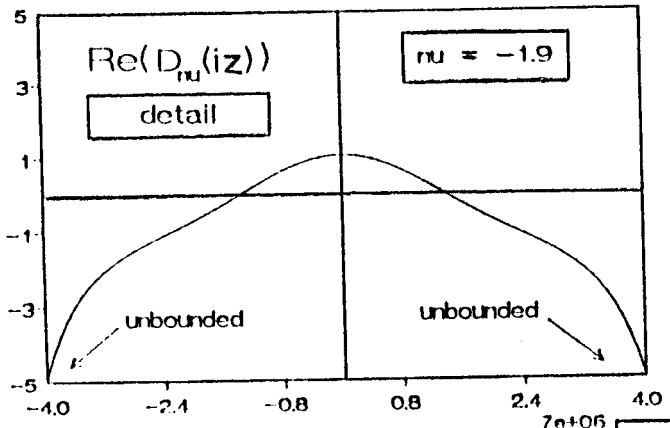

Fig. A3

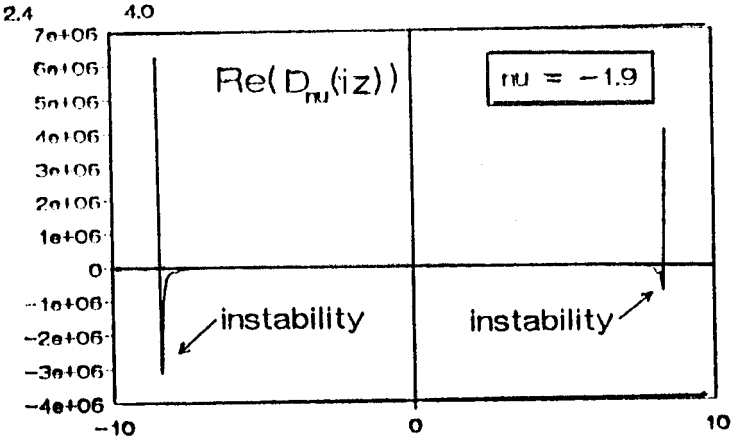

Figures A1, A2, and A3, showing the problems one encounters in calculating the parabolic cylinder functions in terms of Kummer functions.

With the help of the recurrence relations described in the previous section most of these problems are solved, but still there are some difficulties for very large z and/or very large ν, because the repetitive applying of the recurrence relation itself becomes numerical instable. The underlying reason for this difficulties is the fact that for noninteger ν, the functions are at least unbound on one side. Apparently for some combinations of ν and z the power series are convergent but the computer has some difficulty in establishing that convergence. In fact when $|z|$ is large enough numerical instabilities will occur at any ν. Therefore we need a good, i.e. numerically stable, asymptotic expansion.

In search of a useful asymptotic expansion we will now systematically discuss the ones provided in the aforementioned textbooks.

In [S&O] the following expansions are mentioned:

$$D_\nu(z) = 2^{\frac{(2+\nu)}{2}} \frac{\exp(-z^2/4)}{\Gamma(-\nu)} \sum_{j=0}^{\infty} \frac{1}{j!} \Gamma\left(\frac{j-\nu}{2}\right) (-z\sqrt{2})^j \qquad (A.18)$$

$$D_\nu(z) = (2^\nu \pi)^{1/2} \exp(z^2/4) \sum_{j=0}^{\infty} \frac{1}{j!} \frac{(-z\sqrt{2})^j}{\Gamma\left(\frac{1-j-\nu}{2}\right)} \qquad (A.19)$$

$$D_\nu(z) = \sqrt{2^\nu/\pi}\ \exp(z^2/4) \sum_{j=0}^{\infty} \cos\left(\frac{\nu\pi+j\pi}{2}\right) \frac{1}{j!} \Gamma\left(\frac{1+j+\nu}{2}\right) (z\sqrt{2})^j \qquad (A.20)$$

and:

$$D_\nu(z) \sim z^\nu \exp(-z^2/4) \left\{ 1 - \frac{(-\nu)(1-\nu)}{2z^2} + \frac{(-\nu)(1-\nu)(2-\nu)(3-\nu)}{2!(2z^2)^2} - \ldots + \frac{(-\nu)_{2j}}{j!(-2z^2)^j} + \ldots \right\} \qquad z \longrightarrow \infty \qquad (A.21)$$

Further, [S&O] gives an algorithm which is said to have a relative accuracy of 6×10^{-8} or better, which may be degraded near the zeros of $D_\nu(z)$ or when z and $-\nu$ are both large and positive. During examining this algorithm it proved to be not as good as is claimed, worse, it already is instable at z

≈ 8 at $\nu = 4.5$. Therefore, this algorithm is not what we are looking for.
In [A&S] the solutions of the parabolic cylinder functions are the aforementioned U(a,z) and V(a,z) (see Eq.(A.12)). Also expressions in power series and Kummer functions/ confluent hypergeometric functions are given. Further, asymptotic expansions for large z and a moderate, a large and z moderate,and Darwin's expansions for a positive and z^2+4a large, a negative and z^2+4a large and positive and, a large and negative and x moderate.
We give here the first two types:

(i) z large and a moderate, when $|z| \gg |a|$,

$$U(a,z) \approx \exp\left(\frac{-z^2}{4}\right) z^{-a-\frac{1}{2}} \left\{ 1 - \frac{(a+\frac{1}{2})(a+\frac{3}{2})}{2z^2} + \frac{(a+\frac{1}{2})(a+\frac{3}{2})(a+\frac{5}{2})(a+\frac{7}{2})}{2\cdot 2z^4} - \ldots \right\}$$
$$(z \longrightarrow \infty) \qquad (A.22)$$

Eq. (A.22) is "valid for complex z with $|\arg z| < \frac{1}{2}\pi$, in the complete sense of Watson, although valid for a wider range of $|\arg z|$ in Poincaré's sense."

(ii) a large and z moderate;
(iia) a positive;
When $a \gg z^2$, with $p = \sqrt{a}$, then:

$$U(a,z) = \frac{\sqrt{a}\, \exp(-pz+\vartheta_1)}{2^{\frac{1}{2}a+\frac{1}{4}}\, \Gamma\left(\frac{3}{4}+\frac{1}{2}a\right)} \qquad U(a,-z) = \frac{\sqrt{a}\, \exp(pz+\vartheta_2)}{2^{\frac{1}{2}a+\frac{1}{4}}\, \Gamma\left(\frac{3}{4}+\frac{1}{2}a\right)} \qquad (A.23)$$

where,

$$\vartheta_1, \vartheta_2 \approx \mp \frac{\frac{2}{3}(\frac{1}{2}z)^3}{2p} - \frac{(\frac{1}{2}z)^2}{(2p)^2} \mp \frac{\frac{1}{2}z-\frac{2}{5}(\frac{1}{2}z)^5}{(2p)^3} + \frac{2(\frac{1}{2}z)^4}{(2p)^4} \pm \frac{(\frac{16}{3}\ \frac{1}{2}z)^3 - \frac{4}{7}(\frac{1}{2}z)^7}{(2p)^5} - \cdots$$
$$(a \longrightarrow +\infty) \qquad (A.24)$$

The upper sign in Eq.(A.24) gives the first function, and the lower sign gives the second function.

(iib) a negative

When $-a \gg z^2$, with $p = \sqrt{-a}$, then

$$U(a,z) + i\,\Gamma(\tfrac{1}{2} - a)\cdot V(a,z) = \frac{\Gamma(\frac{1}{4} - \frac{1}{2})}{2^{\frac{1}{2}a+\frac{1}{4}}\sqrt{\pi}}\, e^{i\pi(\frac{1}{4}+\frac{1}{2}a)}\, e^{ipz}\, e^{(\wp_r + i\wp_i)} \qquad (A.25)$$

where

$$\wp_r \approx + \frac{(\frac{1}{2}z)^2}{(2p)^2} + \frac{2(\frac{1}{2}z)^4}{(2p)^4} - \frac{9(\frac{1}{2}z)^2 - \frac{16}{3}(\frac{1}{2}z)^6}{(2p)^6} - \ldots \qquad (A.26)$$

$$\wp_i \approx - \frac{\frac{2}{3}(\frac{1}{2}z)^3}{2p} + \frac{\frac{1}{2}z + \frac{2}{5}(\frac{1}{2}z)^5}{(2p)^3} + \frac{\frac{16}{3}(\frac{1}{2}z)^3 - \frac{4}{7}(\frac{1}{2}z)^7}{(2p)^5} - \ldots \qquad (A.27)$$

Here we conclude our bird's-eye-view of the asymptotic expansions discussed in [A&S] and continue with [EMOT].

They use the same notation as [S&O] and are more specific about the arguments of the complex z in $D_\nu(z)$ because that has great influence on the type of asymptotic expansion:

$$D_\nu(z) = z^\nu \exp\left(\frac{-z^2}{4}\right)\left[\sum_{n=0}^{N} \frac{(-\frac{1}{2}\nu)_n (\frac{1}{2}-\frac{1}{2}\nu)_n}{n!(-\frac{1}{2}z^2)^n} + O|z^2|^{-N-1}\right] \quad -\tfrac{3}{4}\pi < \arg z < \tfrac{3}{4}\pi \qquad (A.28)$$

$$D_\nu(z) = z^\nu \exp\left(\frac{-z^2}{4}\right)\left[\sum_{n=0}^{N} \frac{(-\frac{1}{2}\nu)_n (\frac{1}{2}-\frac{1}{2}\nu)_n}{n!(-\frac{1}{2}z^2)^n} + O|z^2|^{-N-1} - \right.$$

$$\frac{(2\pi)^{1/2}}{\Gamma(-\nu)}\, e^{\nu\pi i}\, z^{-\nu-1} \exp\left(\frac{z^2}{4}\right) \left.\sum_{n=0}^{N} \frac{(\frac{1}{2}\nu)_n (\frac{1}{2}+\frac{1}{2}\nu)_n}{n!(\frac{1}{2}z^2)^n} + O|z^2|^{-N-1}\right]$$

$$\frac{\pi}{4} < \arg z < \frac{5\pi}{4} \qquad (A.29)$$

and:

$$D_\nu(z) = z^\nu \exp\left(\frac{-z^2}{4}\right) \left[\sum_{n=0}^{N} \frac{(-\frac{1}{2}\nu)_n (\frac{1}{2}-\frac{1}{2}\nu)_n}{n!(-\frac{1}{2}z^2)^n} + O|z^2|^{-N-1} - \right.$$

$$\left. \frac{(2\pi)^{1/2}}{\Gamma(-\nu)} e^{-\nu\pi i} z^{-\nu-1} \exp\left(\frac{z^2}{4}\right) \sum_{n=0}^{N} \frac{(\frac{1}{2}\nu)_n (\frac{1}{2}+\frac{1}{2}\nu)_n}{n!(\frac{1}{2}z^2)^n} + O|z^2|^{-N-1} \right]$$

$$\frac{-5\pi}{4} < \arg z < \frac{-\pi}{4} \qquad \text{(A.30)}$$

In these the notation $(a)_0 = 1$, $(a)_n = a(a+1)\ldots(a+n-1)$, $n = 1,2,3,..$ is used. Note that the last two expansions only differ on one place, indicated with arrows. We will compare these expansions with ones discussed in [BH]. Because we are interested in argz = 0 and argz = $\pm\frac{1}{2}\pi$, we need all three of the expansions. Up till now [EMOT] gives the most general asymptotic expansions, with respect to the argument of z. To check these expressions we use the asymptotic expansions described in [BH] at page 92:

$$D_\nu(z) \sim z^\nu e^{-z^2/4} \left\{ \sum_{\lambda=0}^{p-1} (-1)^\lambda \frac{(-\nu)_{2\lambda}}{\lambda!} (2^{1/2}z)^{-2\lambda} + O(z^{-2p}) \right\}, \quad |\arg z| < \frac{3\pi}{4} \qquad \text{(A.31)}$$

$$D_{-\nu-1}(\pm iz) \sim z^{-\nu-1} e^{\frac{z^2}{4} \mp \frac{\pi i(1+\nu)}{2}} \left\{ \sum_{\lambda=0}^{p-1} \frac{(\nu+1)_{2\lambda}}{\lambda!} (2^{1/2}z)^{-2\lambda} + O(z^{-2p}) \right\} \qquad \text{(A.32)}$$

In Eq.(A.32), the upper sign gives an expansion for $-\frac{5\pi}{4} < \arg z < \frac{\pi}{4}$, which is useful for argz = $-\frac{1}{2}\pi$ values of z, whereas the lower sign yields an expansion for $-\frac{\pi}{4} < \arg z < \frac{5\pi}{4}$, useful for the options argz equals 0 or $\frac{1}{2}\pi$. Equations (A.31) and (A.32) are in agreement with Eq. (A.28), (A.29), (A.30). Our last reference is [MB], in which the parabolic cylinder functions emerge when the double oscillator is discussed. However, [MB] doesn't give an expansion for the complex z case. The only expansion [MB] gives is identical to (A.29). The best expansions to use are (A.31) and (A.32). In combination with the recurrence relations it is possible to determine the value of the parabolic cylinder function in reasonable ranges of z and ν.

A.6. Finally

Because it seemed simple to devise an algorithm which could fast and accurate determine the wave functions in our DBRT structure, this study has been made. However, all kinds of numerical problems emerged, resulting in a last attempt which failed dramatically. This last attempt consisted of using the fortran77 subroutines DIMACH and DCHU, made by W. Fullerton of the Los Alamos Scientific Laboratory. It appeared, after being sent over from the U.S.A., that these routines only worked on a very limited interval of parameters. Because we had reached by that stage another insight in the modeling of the DBRT, we abandoned the parabolic cylinder function.

APPENDIX B: THE TRANSFER MATRIX FORMALISM.

B.1. Introduction

In this appendix we discuss the Transfer Matrix Formalism, which proves to be an excellent tool for dealing with boundary conditions. For instance, we know that because of conservation of probability in the B = 0 case, the boundary conditions are continuity of wave function and continuity of the gradient of the wave function. When the solutions of the Schrödinger equations in the different regions (different potential energies) are known, the total wave function is composed out of the separate solutions by means of the boundary conditions.
We will first describe the general matrix formalism and then confine ourselves to the description of the Matrix Formalism we applied on the DBRT structure under transverse magnetic field. We will discuss the different structures of the device matrix which tells us whether the electron is able to participate in the current through our DBRT structure, or whether the electron is (quasi or truly) caught in the well.

B.2. General Matrix Formalism.

Consider two regions separated by an interface at $z = \xi$. The region on the left ($z < \xi$) will be called region m and the region on the right ($z > \xi$) will be called region m+1. Suppose we have found the complete set of solutions of a certain equation in both regions:

$$\text{region m:} \quad \langle f_1, f_2, f_3, .. \rangle \qquad \text{region m+1:} \quad \langle g_1, g_2, g_3, .. \rangle \tag{B.1}$$

So, a general solution in region m , respectively m+1 can be written as:

$$\Psi_m(z) = \sum_{j=1}^{\infty} C_j f_j(z) \qquad \Psi_{m+1}(z) = \sum_{j=1}^{\infty} D_j g_j(z) \qquad C_j \text{ and } D_j \text{ constants} \tag{B.2}$$

Suppose, the boundary conditions at $z = \xi$ are continuity of Ψ and continuity of its gradient:

$$\sum_{j=1}^{\infty} C_j f_j(\xi) = \sum_{j=1}^{\infty} D_j g_j(\xi) \qquad \text{and:} \qquad \sum_{j=1}^{\infty} C_j f_j'(\xi) = \sum_{j=1}^{\infty} D_j g_j'(\xi) \tag{B.3}$$

These two equations can be written as a matrix equation, which connects the vector in basis $<g_j>$ to the vector in basis $<f_j>$ by a matrix which contains the values $f_j(\xi)$, $f_j'(\xi)$, $g_j(\xi)$, and $g_j'(\xi)$ in certain combinations. As an example, consider the bases left and right of the interface to be $<f_1(z),f_2(z)>$ and $<g_1(z),g_2(z)>$, so that the connection rules are:

$$\begin{pmatrix} f_1(\xi) & f_2(\xi) \\ f_1'(\xi) & f_2'(\xi) \end{pmatrix} \cdot \begin{pmatrix} C_1 \\ C_2 \end{pmatrix} = \begin{pmatrix} g_1(\xi) & g_2(\xi) \\ g_1'(\xi) & g_2'(\xi) \end{pmatrix} \cdot \begin{pmatrix} D_1 \\ D_2 \end{pmatrix} \tag{B.4}$$

which we can rewrite as (with $f_j'=f_j'(\xi)$ and $g_j'=g_j'(\xi)$ etc.):

$$\begin{pmatrix} D_1 \\ D_2 \end{pmatrix} = M_m^{m+1} \begin{pmatrix} C_1 \\ C_2 \end{pmatrix}, \text{ with } M_m^{m+1} = \frac{1}{g_1 g_2' - g_2 g_1'} \begin{pmatrix} f_1 g_2' - f_1' g_2 & f_2 g_2' - f_2' g_2 \\ f_1' g_1 - f_1 g_1' & f_2' g_1 - f_2 g_1' \end{pmatrix} \tag{B.5}$$

Thus we can easily consider n interfaces after each other. The total matrix M transforms the vector on the outer left to the vector on the outer right:

$$\begin{pmatrix} \Lambda_1 \\ \Lambda_2 \end{pmatrix}_{\text{right}} = M_{n-1}^{n} \cdots M_m^{m+1} \cdots M_1^{2} \begin{pmatrix} \Xi_1 \\ \Xi_2 \end{pmatrix}_{\text{left}} \tag{B.6}$$

Dependent on the set basis functions, the matrix M shows sometimes remarkable features. For instance, when dealing with the basis consisting of functions that are complex conjugated with respect to each other (such as exp(ikz) and exp(-ikz)), the matrix M has the following form:

$$M = \begin{pmatrix} \mathcal{M}_{11} & \mathcal{M}_{12} \\ \mathcal{M}_{12}^* & \mathcal{M}_{11}^* \end{pmatrix} \tag{B.7}$$

We call this matrix form current carrying, as will become clear in the next section were the general matrix formalism is applied with a basis of plane waves on a Double Barrier Resonant Tunneling Structure.

B.3. The DBRT-structure with a transverse magnetic field.

In the chapter 3 we saw that in our model the wave functions that are the solutions of the Schrödinger equation with gauge $\underline{A}$ = (0,-Bz,0) are modeled as plane waves. Further, in our model we only consider tunneling from left to right, so that it is handy to perform the transfer matrix formalism in the opposite way: on the right hand side of the structure we take only an outgoing wave, namely $\exp(ik_{zright}z)$. The matrix defined in section *A.2* has to be inverted to apply on this configuration. This means that in this view current carrying matrix has also the form of Eq.(B.7).
The only difference with the B=0 case lies in the fact that now the transmission probability depends not only for each k_z but also for each k_y. Further, the boundary conditions are different from Eq. (B.4) because the momentum in the y-direction, k_y, can change suddenly when passing an interface (See section 2.3 of the report).
This all means that at an interface we have to glue the following wave functions according the boundary conditions (left and right of the interface respectively):

$$\Psi_{left} = \exp(ik_x x + ik_{y1} y)\cdot\left(C_1\exp(ik_{z1}z)+C_2\exp(-ik_{z1}z)\right) \tag{B.8}$$

$$\Psi_{right} = \exp(ik_x x + ik_{y2} y)\cdot\left(C_3\exp(ik_{z2}z)+C_4\exp(-ik_{z2}z)\right) \tag{B.9}$$

Suppose the interface lies at $z=\xi$, then according to the boundary conditions described in the Chapter 2. Suppose the magnetic field is zero in the left region and non-zero in the right:

$$k_{y1} = k_{y2} - \frac{e\xi B}{\hbar} \tag{B.10}$$

Thus the boundary conditions for the two wave functions (B.8) and (B.9) are:

$$\exp(ik_x x+i\left(k_{y2} - \frac{e\xi B}{\hbar}\right)y)\cdot\left(C_1\exp(ik_{z1}\xi)+C_2\exp(-ik_{z1}\xi)\right) =$$

$$\exp(ik_x x+ik_{y2}y)\cdot\left(C_3\exp(ik_{z2}\xi)+C_4\exp(-ik_{z2}\xi)\right) \qquad \text{(B.11)}$$

$$\exp(ik_x x+i\left(k_{y2} - \frac{e\xi B}{\hbar}\right)y)\cdot\left(C_1 ik_{z1}\exp(ik_{z1}\xi)-C_2 ik_{z1}\exp(-ik_{z1}\xi)\right) =$$

$$\exp(ik_x x+ik_{y2}y)\cdot\left(C_3 ik_{z2}\exp(ik_{z2}\xi)-C_4 ik_{z2}\exp(-ik_{z2}\xi)\right) \qquad \text{(B.12)}$$

The values of k_{z1} is not important, they can be real or imaginary dependent on the fact whether the kinetic energy $\hbar^2k_z^2/2m$ in the z-direction is positive or negative. From Eq. (B.11) and (B.12) we learn that the fact that the k_y changes is no obstruction for performing Transfer Matrix Formalism, as long as we keep in mind what basis of functions we are working in. In fact, k_y changes only when the magnetic field changes, which is only two times in the whole structure. In fig.B.1 the value of k_y is shown throughout the structure.

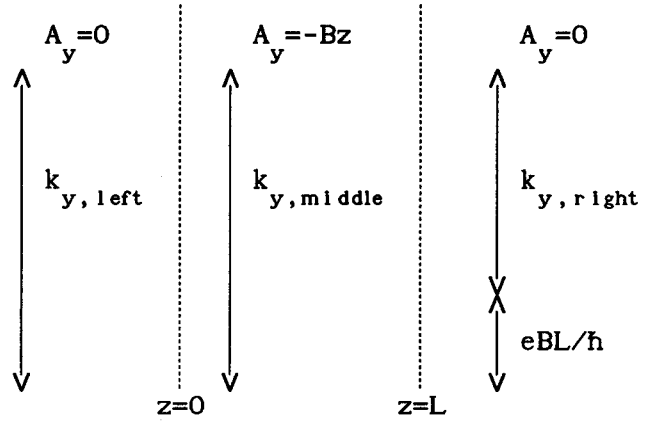

Figure B.1 The value of k_y changes when the vector potential is discontinuous. In this example we used the choice of gauge described in chapter 2.

The fact that we have to deal with changing momenta in the y-direction is one of the changes a transverse magnetic field imposes on calculating the wave function.
When a number of interfaces is considered, the total matrix can be calculated by a repetitive procedure which led to to the matrix for one interface. The wave functions on the right of the first interface serve as the incoming waves at the next interface. In [14] this is more elaborately described with matrices for the two barriers and a translation matrix for the well.
In the B=0 case we saw that whenever an electron had the resonance energy, it took part in the resonant current and therefore the total matrix was current carrying. In the non-zero field case, this is not always true: when an electron has an energy such that it tunnels into the level in the well, the second barrier may be impenetrable. We then say that the electron is in a quasi-bound state; it can only escape from the well by tunneling back to where it came from.
Another possibility is that the electron is in the well, but it can't escape from it. We then say the electron is in a bound state. In our model this event doesn't occur because it implies coherence destroying processes: the electron will have to lose energy to get below both the band minima on the left and the right of the structure. This can happen for instance when a electron tunnels non-resonantly into the well, looses energy by phonon interaction and is caught in the well. This is why with a transverse magnetic field charge build-up in the well can be very important.
It is obvious that these three situations have different transfer matrices. In the next section we will discuss these three forms briefly.

B.4. The three device matrix types

B.4.1 The current carrying type.

This type has been discussed thoroughly in [14], so here we will keep it short. Whenever a matrix is composed which describes the gluing of on one side an incoming and reflecting wave and on the other side an outgoing wave the matrix will be current carrying, no matter what obscure functions have to be used in the region between them. The result will always be (with only

an outgoing wave on the right hand side of the structure and with ρ and τ the complex reflection coefficient and the complex transmission coefficient respectively:

$$\begin{matrix} & & 1^{st}\text{ barrier} & & \text{well} & & 2^{nd}\text{ barrier} \end{matrix}$$

$$\begin{pmatrix} 1 \\ \rho^{*}\tau/\tau^{*} \end{pmatrix} = \begin{pmatrix} B_{111} & B_{112} \\ B^{*}_{112} & B^{*}_{111} \end{pmatrix} \cdot \begin{pmatrix} e^{-ik_w L_w} & 0 \\ 0 & e^{ik_w L_w} \end{pmatrix} \cdot \begin{pmatrix} B_{211} & B_{212} \\ B^{*}_{212} & B^{*}_{211} \end{pmatrix} \cdot \begin{pmatrix} \tau \\ 0 \end{pmatrix}$$

$$= \begin{pmatrix} 1/\tau & \rho/\tau \\ \rho^{*}/\tau^{*} & 1/\tau^{*} \end{pmatrix} \cdot \begin{pmatrix} \tau \\ 0 \end{pmatrix} \qquad \text{(B.13)}$$

Eq. (B.13) describes what combination of incoming/reflecting waves, $\exp(ikz) + \rho^{*}\tau/\tau^{*}\exp(-ikz)$, is needed to get an outgoing wave $\tau \cdot \exp(ikz)$.
A resonant state is characterized by a maximum in the coefficient of the outgoing wave, which is equal to τ. This is maximal when the following condition is valid:

$$\gamma_{res} = 2k_w L_w + \arg\left(\frac{B_{112} \cdot B^{*}_{212}}{B_{111} \cdot B^{*}_{211}} \right) = (N+\tfrac{1}{2})\, 2\pi \qquad \text{(B.14)}$$

Because we only deal with one level, so only one γ_{res}, this equation is very handy in calculating the charge density in the well, which will be discussed in the next chapter.

B.4.2 The Quasi-Bound state type.

This type will be encountered when one of the matrices for the barriers is not current carrying. In our model it is logical to confine this to the case that the second barrier is impenetrable because the potential energy on the right hand side of the structure is larger than the electrons kinetic energy.
Therefore, the total matrix will be composed as follows:

$$\underline{\underline{D}} = \underline{\underline{B}}_1 \cdot \underline{\underline{\Lambda}} \cdot \underline{\underline{B}}_2 = \begin{pmatrix} B_{111} & B_{112} \\ B^*_{112} & B^*_{111} \end{pmatrix} \cdot \begin{pmatrix} e^{-ik_w L_w} & 0 \\ 0 & e^{ik_w L_w} \end{pmatrix} \cdot \begin{pmatrix} B_{211} & B_{212} \\ B^*_{211} & B^*_{212} \end{pmatrix} \qquad \text{(B.15)}$$

In Eq.(B.14) it is clear that the last matrix on the right hand side is not current carrying; it describes the linking of plane waves in the well to exponentially damped functions. When k_z becomes imaginary the condition for current carrying matrices is violated: $\exp(-\kappa z)$ is not the complex conjugate of $\exp(\kappa z)$. As a result of this the total matrix has the following form (with $e^{\pm}$ for $\exp(\pm ik_w L_w)$):

$$\underline{\underline{D}} = \begin{pmatrix} B_{111}e^{-}B_{211}+B_{112}e^{+}B^*_{211} & B_{111}e^{-}B_{212}+B_{112}e^{+}B^*_{212} \\ B^*_{112}e^{-}B_{211}+B^*_{111}e^{+}B^*_{211} & B^*_{112}e^{-}B_{212}+B^*_{111}e^{+}B^*_{212} \end{pmatrix} = \begin{pmatrix} D_{11} & D_{12} \\ D^*_{11} & D^*_{12} \end{pmatrix} \qquad \text{(B.16)}$$

We can compose a condition which expresses at what circumstances we deal with maximum probability in the well, similar to Eq.(B.14). Therefore we look at the amplitude of the wave in the well:

$$\Psi_{well} = \varepsilon \exp(ik_w z) + \eta \exp(-ik_w z) \qquad \text{(B.17)}$$

In Eq.(B.17) the coefficients ε and η are dependent of the various matrix elements via:

$$\varepsilon = \frac{B_{211}}{D_{11}} \exp(-ik_w(L_1+L_w)) \quad , \quad \eta = \frac{B^*_{211}}{D_{11}} \exp(ik_w(L_1+L_w)) \qquad \text{(B.18)}$$

In Eq.(B.18) L_1 is the width of the first barrier and L_w the width of the well. The amplitude of the wave function in the well is maximal when the matrix element D_{11} is minimal. So the Quasi-Bound-State condition reads:

$$\gamma_{QBS} = 2k_w L_w + \arg\left(\frac{B_{112} \cdot B^*_{211}}{B_{111} \cdot B_{211}} \right) = (N+\tfrac{1}{2})\, 2\pi \qquad \text{(B.19)}$$

Comparing this with Eq.(B.14), we see that the same matrix elements are

involved, only with a different name.

B.4.3 The Bound state type.

The last type we will discuss is the type that one encounters when, for some reason, there is charge in the well. When the conduction band minima on either sides of the structure lie higher than the energy of the electron, the electron is truly bound in the well The "transfer" matrix connects two damped functions, one in front of the first barrier and one after the second barrier, by means of a standing wave in the well. This matrix will look like:

$$\underline{\underline{D}} = \underline{\underline{B}}_1^{-1} \cdot \underline{\underline{\Lambda}} \cdot \underline{\underline{B}}_2 = \begin{pmatrix} B_{111} & B_{111}^* \\ B_{121} & B_{121}^* \end{pmatrix} \cdot \begin{pmatrix} e^{-ik_w L_w} & 0 \\ 0 & e^{ik_w L_w} \end{pmatrix} \cdot \begin{pmatrix} B_{211} & B_{212} \\ B_{211}^* & B_{212}^* \end{pmatrix}$$

$$= \left(\begin{array}{c|c} B_{111}e^{-}B_{211} + \text{c.c.} & B_{111}e^{-}B_{212} + \text{c.c.} \\ \hline B_{121}e^{-}B_{211} + \text{c.c.} & B_{121}e^{-}B_{212} + \text{c.c.} \end{array} \right) \qquad \text{(B.20)}$$

So that:

$$\begin{pmatrix} \lambda \\ 0 \end{pmatrix} = \begin{pmatrix} D_{11} & D_{12} \\ D_{21} & D_{22} \end{pmatrix} \cdot \begin{pmatrix} \mu \\ 0 \end{pmatrix} \qquad \text{(B.21)}$$

In search of a condition for a bound state we see that $D_{21} = 0$ to keep the solutions under control. In terms of arguments of the various matrix elements this condition reads:

$$2k_w L_w - 2\arg(B_{121}) - 2\arg(B_{211}) = (N+\tfrac{1}{2})\,2\pi \quad , N \in \mathbb{Z} \qquad \text{(B.22)}$$

We can also look at the amplitude of the wave function in the well and find out when that is maximal. It appears to be maximal when D_{11} is minimal, which yields another condition:

$$2k_w L_w - 2\arg(B_{111}) - 2\arg(B_{211}) = (N+\tfrac{1}{2})\,2\pi \quad , N \in \mathbb{Z} \qquad \text{(B.23)}$$

Comparing the last two conditions leads to the conclusion that apparently when the electron is in a bound state the arguments of B_{111} and B_{121} must be the same.

The conditions described in this section facilitate the finding of the energy level in the well when that is unknown or changing.

In the next chapter we will thoroughly describe how the charge density in the well is calculated with the help of this transfer matrix formalism.

APPENDIX C: THE CALCULATION OF CHARGE- AND CURRENT- DENSITIES.

C.1 Introduction

In this appendix we will describe how the charge densities, specifically the one in the well, and the current density are calculated in our FORTRAN77 program. It is similar to Joosten's section 7.13 [14] with a few differences.

First of all we will discuss the transition from summation to integral which is only possible when periodic boundary conditions are assumed. Then we will, with the help of the results of the chapter about the transfer matrix formalism, derive an analytical expression for the integral over the kinetic energy. Finally we will implement these results in an expression for the current density.

C.2 The charge density in the left spacer.

The general way to calculate a charge density is to count all electrons in a volume and to divide the result by this volume. Because we are dealing with quantum mechanics we have to take probability and distribution into account (where are the electrons and how many are there?). Thus the wave function and the Fermi-Dirac distribution function are needed to calculate the electron density at position z:

$$n_3(z) = g_s \sum_{k_x} \sum_{k_y} \sum_{k_z} |\Psi(\underline{k},\underline{r})|^2 \, f_{FD}(E(\underline{k})) \qquad \text{(C.1)}$$

The wave function Ψ must be appropriately normalized. When calculating the electron density in the well, the right value of Ψ is the mean value of the envelope function in the well. When calculating the electron density in the left spacer, the value of Ψ at the beginning of the first barrier is an underestimation because the wave function penetrates the barrier a little. Therefore one has to be careful in choosing the Ψ in Eq.(C.1).

The summations over the wave numbers can be transformed with the help of periodic boundary conditions, that demand that the wave numbers k_x, k_y and

k_z are such that:

$$L_i = n \frac{2\pi}{k_i} \qquad n \in \mathbb{N} \ , \ i=x,y,z \tag{C.2}$$

When the dimensions L_i are large enough we can change the summations into integrals with:

$$\frac{1}{L_i} \sum_{k_x} \longrightarrow \frac{1}{2\pi} \int dk_i \tag{C.3}$$

Because in Eq.(C.1) the wave function is appropriately normalized, the dimensions L_i disappear from the equations.
Before calculating the charge density in the left spacer, n_{3sp}, we note that for typical situations the reflection probability R_D is very near to one, even for the resonant channel, so the following approximation will not introduce a large error:

$$\left| \exp(ik_x x) \cdot \exp(ik_y y) \cdot \left(\exp(ik_z z) + R_D \exp(-ik_z z) \right) \right|^2 \cong 2 \tag{C.4}$$

Thus the integral for the charge density in front of the first barrier looks like:

$$n_{3sp} = g_s \frac{1}{8\pi^3} \int\int\int dk_x dk_y dk_z \cdot 2 \cdot f_{FD}(E(\underline{k})) \tag{C.5}$$

Because the magnetic field is confined to the barriers and the well, we don't have to perform the integration over k_y separate from the other two. With a change of variables, from $dk_x dk_y dk_z$ to dE, the integrals in Eq.(C.5) can be written as a Fermi-Dirac integral of order 1/2 [15]. These Fermi-Dirac integrals are the moments of the Fermi-Dirac distribution:

$$\mathfrak{F}_j(\eta) = \frac{\beta^{j+1}}{\Gamma(j+1)} \int dE \ E^j f_{FD}(E) = \frac{1}{\Gamma(j+1)} \int d\varepsilon \ \frac{\varepsilon^j}{1+\exp(\varepsilon-\eta)} \qquad \beta = \frac{1}{k_B T} \tag{C.6}$$

The result is a simple expression for the charge density in the left

spacer:

$$n_{3sp} = e\, g_s \left(\frac{m}{2\pi\hbar^2\beta} \right)^{3/2} \mathfrak{F}_{1/2}(\beta E_F) \qquad (C.7)$$

In our model this three dimensional density is modeled as a two dimensional one in order to get a kink in the potential energy. This is done by multiplying Eq.(C.7) by the width of the left spacer, L_{sp}, which is about 28.3 Å. The spacer is the first undoped layer from the structure, so it's the first region where the charge of the electrons isn't compensated by the donor atoms. In the next section we will describe the procedure for calculating the electron density in the well.

C.3 The charge density in the well

The calculation of the charge density in the well when a transverse magnetic field is present is different from the nonzero field case because we cannot perform the integral over k_y analytically. Further, it is somewhat different from the calculation of n_{3sp} because approximation (5.4) is not realistic anymore. This is obvious when we look at the wave function in the well:

$$\Psi(z) = \frac{\eta_{11}}{D_{11}} \exp(ik_w z) + \frac{\eta_{21}}{D_{11}} \exp(-ik_w z) \qquad (C.8)$$

The complex numbers η_{11}, η_{21} and D_{11} are complex matrix elements: η_{ij} represents the matrix of the second barrier and D_{ij} denotes the total matrix of the structure. The mean value of the wave function in the well is calculated by:

$$\frac{1}{L_w}\int_{L_1}^{L_1+L_w} dz\ |\Psi(z)|^2 = \frac{1}{|D_{11}|^2}\left(|\eta_{11}|^2 + |\eta_{21}|^2 + \right.$$

$$\left. + \eta_{11}\eta_{21}^* \frac{e^{2ik_w(L_1+L_w)} - e^{2ik_w L_w}}{2ik_w L_w} - \eta_{11}^*\eta_{21} \frac{e^{-2ik_w(L_1+L_w)} - e^{-2ik_w L_w}}{2ik_w L_w} \right) \quad \text{(C.9)}$$

The factor between brackets is a smooth function of the electron energy; the peaked behavior is caused by the term $1/|D_{11}|^2$. In Eq.(C.9), L_1 is the width of the first barrier, L_w is the width of the well, k_w is the wave number in the well and η_{ij} and D_{ij} are the aforementioned matrix elements, which are expressed in the different wave numbers of the electron in the following way (k_i is the complex wave number in region i, regions 2 and 4 are the first and second barrier respectively, regions 1 and 5 are the left and right spacer and region 3 is the well):

<u>first barrier:</u>

$$(B_{ij}) = \begin{pmatrix} B_{11} & B_{12} \\ B_{21} & B_{22} \end{pmatrix} \quad \text{(C.10)}$$

$$4B_{11} = \left(1 + \frac{ik_2}{ik_1}\right)\left(1 + \frac{ik_3}{ik_2}\right) e^{i(k_3-k_2)L_1} + \left(1 - \frac{ik_2}{ik_1}\right)\left(1 - \frac{ik_3}{ik_2}\right) e^{i(k_3+k_2)L_1}$$

$$4B_{12} = \left(1 + \frac{ik_2}{ik_1}\right)\left(1 - \frac{ik_3}{ik_2}\right) e^{-i(k_3+k_2)L_1} + \left(1 - \frac{ik_2}{ik_1}\right)\left(1 + \frac{ik_3}{ik_2}\right) e^{-i(k_3-k_2)L_1}$$

$$4B_{21} = \left(1 - \frac{ik_2}{ik_1}\right)\left(1 + \frac{ik_3}{ik_2}\right) e^{i(k_3-k_2)L_1} + \left(1 + \frac{ik_2}{ik_1}\right)\left(1 - \frac{ik_3}{ik_2}\right) e^{i(k_3+k_2)L_1}$$

$$4B_{22} = \left(1 - \frac{ik_2}{ik_1}\right)\left(1 - \frac{ik_3}{ik_2}\right) e^{-i(k_3+k_2)L_1} + \left(1 + \frac{ik_2}{ik_1}\right)\left(1 + \frac{ik_3}{ik_2}\right) e^{-i(k_3-k_2)L_1} \quad \text{(C.11)}$$

<u>second barrier:</u>

$$(\eta_{ij}) = \begin{pmatrix} \eta_{11} & \eta_{12} \\ \eta_{21} & \eta_{22} \end{pmatrix} \quad \text{(C.12)}$$

$$4\eta_{11} = \left(1 + \frac{ik_4}{ik_3}\right)\left(1 + \frac{ik_5}{ik_4}\right) e^{i(k_5-k_4)(L_1+L_w+L_2)} e^{i(k_4-k_3)(L_1+L_w)} +$$

$$+ \left(1 - \frac{ik_4}{ik_3}\right)\left(1 - \frac{ik_5}{ik_4}\right) e^{i(k_5+k_4)(L_1+L_w+L_2)} e^{-i(k_4+k_3)(L_1+L_w)}$$

$$4\eta_{12} = \left(1 + \frac{ik_4}{ik_3}\right)\left(1 - \frac{ik_5}{ik_4}\right) e^{-i(k_5+k_4)(L_1+L_w+L_2)} e^{i(k_4-k_3)(L_1+L_w)} +$$

$$+ \left(1 - \frac{ik_4}{ik_3}\right)\left(1 + \frac{ik_5}{ik_4}\right) e^{-i(k_5-k_4)(L_1+L_w+L_2)} e^{-i(k_4+k_3)(L_1+L_w)}$$

$$4\eta_{21} = \left(1 - \frac{ik_4}{ik_3}\right)\left(1 + \frac{ik_5}{ik_4}\right) e^{i(k_5-k_4)(L_1+L_w+L_2)} e^{i(k_4+k_3)(L_1+L_w)} +$$

$$+ \left(1 + \frac{ik_4}{ik_3}\right)\left(1 - \frac{ik_5}{ik_4}\right) e^{i(k_5+k_4)(L_1+L_w+L_2)} e^{-i(k_4-k_3)(L_1+L_w)}$$

$$4\eta_{22} = \left(1 - \frac{ik_4}{ik_3}\right)\left(1 - \frac{ik_5}{ik_4}\right) e^{-i(k_5+k_4)(L_1+L_w+L_2)} e^{i(k_4+k_3)(L_1+L_w)} +$$

$$+ \left(1 + \frac{ik_4}{ik_3}\right)\left(1 - \frac{ik_5}{ik_4}\right) e^{-i(k_5-k_4)(L_1+L_w+L_2)} e^{-i(k_4-k_3)(L_1+L_w)} \qquad \text{(C.13)}$$

Total Device Matrix: $$(D_{ij}) = (B_{ij}) \cdot (\eta_{ij}) = \begin{pmatrix} B_{11} & B_{12} \\ B_{21} & B_{22} \end{pmatrix} \cdot \begin{pmatrix} \eta_{11} & \eta_{12} \\ \eta_{21} & \eta_{22} \end{pmatrix} \qquad \text{(C.14)}$$

$$D_{11} = B_{11}\eta_{11} + B_{12}\eta_{21} \qquad \text{etc.} \qquad \text{(C.15)}$$

Resonances occur when $|D_{11}|^2$ is minimal, that is when:

$$\frac{1 + R_1R_2 + 2(R_1R_2)^{1/2}\cos\gamma}{T_1\Theta_2} \text{ is minimal, with } R_1 = \left|\frac{B_{12}}{B_{11}}\right|^2,\ R_2 = \left|\frac{\eta_{12}}{\eta_{11}}\right|^2,$$

$$T_1 = |B_{11}|^{-2},\ \Theta_2 = |\eta_{11}|^{-2},\ \gamma = \arg\left(\frac{B_{12}\eta_{21}}{B_{11}\eta_{11}}\right) \qquad \text{(C.16)}$$

Θ_2 is the transmission coefficient of the second barrier, provided that the total device matrix is current carrying, otherwise one can not speak of transmission. A resonant or quasi-bound state is found when γ is equal to $(N+\frac{1}{2})\pi$, with N an integer.

Thus we have found an integral expression for the electron density in the well:

$$n_{3w} = g_s \frac{1}{8\pi^3} \int_{-\infty}^{\infty} dk_y \int_{-\infty}^{\infty} dk_z \int_{-\infty}^{\infty} dk_x \quad |\Psi(\underline{k},\underline{r})|^2 \, f_{FD}(E(\underline{k})) \tag{C.17}$$

The integral over k_x is very simple to perform because only the Fermi-Dirac distribution function depends on k_x. The integral over k_z can be performed analytically because we modeled the wave function as a delta-like function. The integral over k_y can not be performed analytically, because all matrix elements are dependent on k_y. Therefore we will perform this integration numerically.

After performing the first integral Eq.(C.17) reads:

$$n_{3w} = g_s \frac{1}{4\pi^3} \left(\frac{m\pi}{2\hbar^2\beta} \right)^{1/2} \int_{-\infty}^{\infty} dk_y \int_{-\infty}^{\infty} dk_z \, |\Psi_w|^2 \, \mathfrak{F}_{-1/2}\Big(\beta(E_{yz}-E_F)\Big) \tag{C.18}$$

where E_{yz} denotes $E-\hbar^2k_x^2/2m$ and $|\Psi_w|^2$ expression (5.8). We now concentrate on the integral over k_z, which contains the resonance:

$$S = \int_{-\infty}^{\infty} dk_z \, |\Psi_w|^2 \, \mathfrak{F}_{-1/2}\Big(\beta(E_{yz}-E_F)\Big) \tag{C.19}$$

Note that k_z is defined in the reservoir. The integral is separated in a resonant and a non-resonant part. The Fermi-Dirac integral with order -1/2 is a well behaving, smooth function of k_z. In a small area around the resonance value of k_z it is in good approximation constant. Because in our model we neglect the non-resonant current the integral S is written as:

$$S = \mathfrak{F}_{-1/2}\Big(\beta(E_{yz}(k_{res})-E_F)\Big) \int_{k_{res}-\Delta k}^{k_{res}+\Delta k} dk_z \, |\Psi_w(k_z)|^2 \tag{C.20}$$

Expression (C.9) is a well behaving smooth function of k_z except the factor

$1/|D_{11}|^2$. With the same procedure as between Eq.(C.19) and (C.20), we get an integral over k_z of $1/|D_{11}|^2$:

$$S = \Im_{-1/2}\left(\beta(E_{yz}-E_F)\right)\ \left((C.9)\right)\Big|_{k_z=k_{res}} \int_{k_{res}-\Delta k}^{k_{res}+\Delta k} dk_z\ |D_{11}|^{-2} \qquad (C.21)$$

where $\left((C.9)\right)$ denotes the term between brackets in (C.9). In Eq.(C.16) we expressed $|D_{11}|^{-2}$ in the variables γ, R_1, R_2, T_1, and Θ_2, so that the integral in Eq.(C.21) reads:

$$S' = \int d\gamma\ \frac{dk_z}{d\gamma}\ \frac{T_1\Theta_2}{1 + R_1R_2 + 2(R_1R_2)^{1/2}\cos\gamma} \qquad (C.22)$$

The factor $dk_z/d\gamma$ is determined numerically by calculating γ for two values of k_z close to the resonance value. With the substitution $\gamma'=\gamma-\pi$, Eq. (C.22) becomes a standard integral, whose solution is found in Gradsteyn [GRAD80] (Equation 2.562), so that the integral S' equals:

$$S' = \frac{2T_1\Theta_2}{1-R^2}\,\pi, \qquad R = R_1R_2 \qquad (C.23)$$

Thus the integration over k_z is analytically performed. (See also [14] section 7.8).

Summarizing, the electron density is calculated by:

$$n_{3w} = \frac{g_s}{4\pi^3}\left(\frac{m\pi}{2\hbar^2\beta}\right)^{1/2}\int_{-\infty}^{\infty} dk_y \left((C.9)\right)_{k_{res}} \cdot \Im_{-1/2}\left(\beta(E_{yz}-E_F)\right)_{k_{res}} \cdot \frac{dk_z}{d\gamma} \cdot \left(\frac{2T_1\Theta_2}{1-R^2}\right)_{k_{res}} \cdot \pi \qquad (C.24)$$

where the integration over k_y is performed numerically. The subscript k_{res} means that the appropriate quantity is calculated with k_z equal to k_{res}, that is in the resonance.

C.4 The resonant current density.

Because we have to consider each k_y separately to calculate the resonant electron density in the well, it is logical to do the same for the resonant current density. For each k_y we calculate the electron density in the well and after that we determine the percentage that has a current carrying matrix for transfer matrix. We determine this by checking whether the electrons concerned can be described by plane waves on either side of the structure.

Thus we calculate for all k_y's considered the resonant current density contribution and add them:

$$J_z = \int_{-\infty}^{+\infty} dk_y \; j_z(k_y) \tag{C.25}$$

The current contributions $j_z(k_y)$ are calculated by the same procedure as in the zero field case; we calculate the non-accumulating charge density in the right spacer, to filter out the electrons at resonance that have an opposite velocity ($-v_{res}$). The resonance velocity involved is:

$$v_{res} = \left(2(E_{res}+V_a+V_w)/m \right)^{1/2} \tag{C.26}$$

In Eq.(C.26), E_{res} is the kinetic energy of the electron concerned in the yz plane, measured from the conduction band minimum on the left of the structure:

$$E_{res} = \frac{\hbar^2}{2m} \left(k_y^2 + k_{res}^2 \right) \tag{C.27}$$

Thus we get for the k_y dependent part of the resonant current density:

$$j_z(k_y) = e \, \mathfrak{D} \, \frac{\sigma_w(k_y)}{L_w} \, \frac{1-R_2(k_y)}{1+R_2(k_y)} \sqrt{2(E_{res}(k_y)+V_a)/m} \tag{C.28}$$

where the electron density in the right spacer is written as a factor

dependent of the transmission probability of the second barrier times the 3D electron density in the well times a factor $\mathfrak{P}$ which is one or zero. It is zero when the transfer matrix for the electrons is not current carrying which means that the resonance level lies below the conduction band minimum of the right spacer. It is one when the transfer matrix is current carrying. This factor $\mathfrak{P}$ is the percentage of electrons that participates in the current.